ACS OMEGA

http://pubs.acs.org/journal/acsodf

Article

# Impact of Minerals and Sealing Systems on the Pore Characteristics of the Qiongzhusi Formation Shale in the Southern Sichuan Basin

Ruiyin Liu, Wen Zhou,* Hao Xu,* Qiumei Zhou, Ke Jiang, Fuhua Shang, Wenlu Gao, Weiguo Song, Dongxu Liu, Hongshuai Zhao, and Xin Zhao

Cite This: *ACS Omega* 2022, 7, 15821−15840

Read Online

ACCESS | Metrics & More | Article Recommendations

**ABSTRACT:** The characteristics, distribution, and preservation of pores are vital in controlling the storage and distribution of shale gas. The Qiongzhusi Formation shales taken from different members with similar tectonic and thermal evolutions were used to evaluate the response of pore characteristics to minerals and sealing systems using field-emission scanning electron microscopy and gas adsorption. Because of differences in mineral structure and arrangement, feldspar, organic matter (OM)−clay, OM−rutile, and OM−apatite aggregates facilitate multiple types of pores in the shale and influence the relative proportions of surface porosity for different types of pores owing to differences in mineral structure and arrangement. Rigid frameworks and pressure shadows formed by rigid minerals and OM−mineral aggregates preserved OM and pores to some extent. The sealing capacity of the floor controls the sealing system and hydrocarbon expulsion efficiency of the Qiongzhusi Formation in different members. During thermal evolution, the amount of hydrocarbons generated and expelled affected the stress equilibrium state between the pore pressure and external stress, influencing the compaction intensity of shales. The OM pore development characteristics were evolved with variation in the stress equilibrium state in different sealing systems. Once the stress equilibrium state was disrupted, the OM pores deformed, narrowed, or even closed under the influence of compaction owing to the loss of overpressure support. The pore characteristics of the Qiongzhusi Formation shales responded significantly to different sealing systems. A few OM pores are flat and slitlike in the open system, whereas numerous OM pores are round and elliptical in the semiopen system. Meanwhile, the average diameter of the OM pores in the open system was reduced by approximately 40.2% compared with that of the semiopen system. Furthermore, the pore volume and specific surface area of the mesopores for open system shales were reduced by 38.4% and 37.7%, respectively, compared to the semiopen system. These findings will improve the understanding of the distribution and preservation of pore in shale and help assess the sweet-spot members for the Qiongzhusi Formation shale gas.

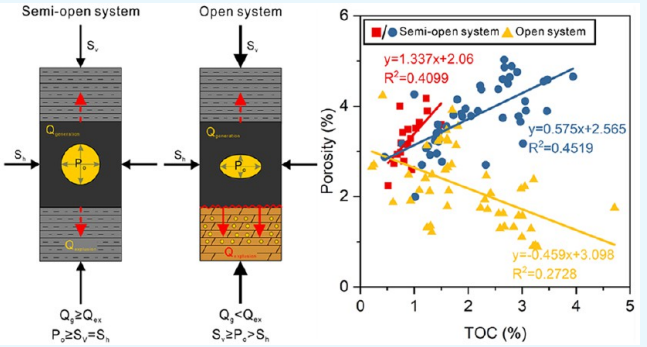


## 1. INTRODUCTION

After more than 10 years of shale gas exploration and development efforts in China, shale gas fields such as Jiaoshiba, Weiyuan, and Changning have been established.[1−3] Currently, there is a growing demand for shale gas as a clean energy source for achieving the goal of carbon neutrality in China. Shale gas exploration and development will gradually shift from the Lower Silurian Longmaxi Formation to other organic-rich shales (e.g., the Lower Cambrian Qiongzhusi or Niutitang Formation and Permian Longtan Formation). Previous studies have shown good potential for shale gas in the Lower Cambrian Qiongzhusi Formation and Lower Silurian Longmaxi Formation.[1,4,5] However, pore development characteristics and shale gas content of the Qiongzhusi Formation differ considerably from those of the Longmaxi Formation.[6] Gas storage and flow in shale are controlled by a heterogeneous pore network,[7−9] which also influences gas and water distribution.[10,11] Therefore, a comprehensive study of the distribution, evolution characteristics, and controlling factors of the pores is necessary to explore and develop the Qiongzhusi Formation shale gas.

The pores in shale are characterized by numerous types, sizes, and shapes due to the complex composition and distribution of minerals.[12] The compaction, cementation, dissolution, and conversion of organic matter (OM) affect

Received: February 14, 2022
Accepted: April 19, 2022
Published: April 28, 2022

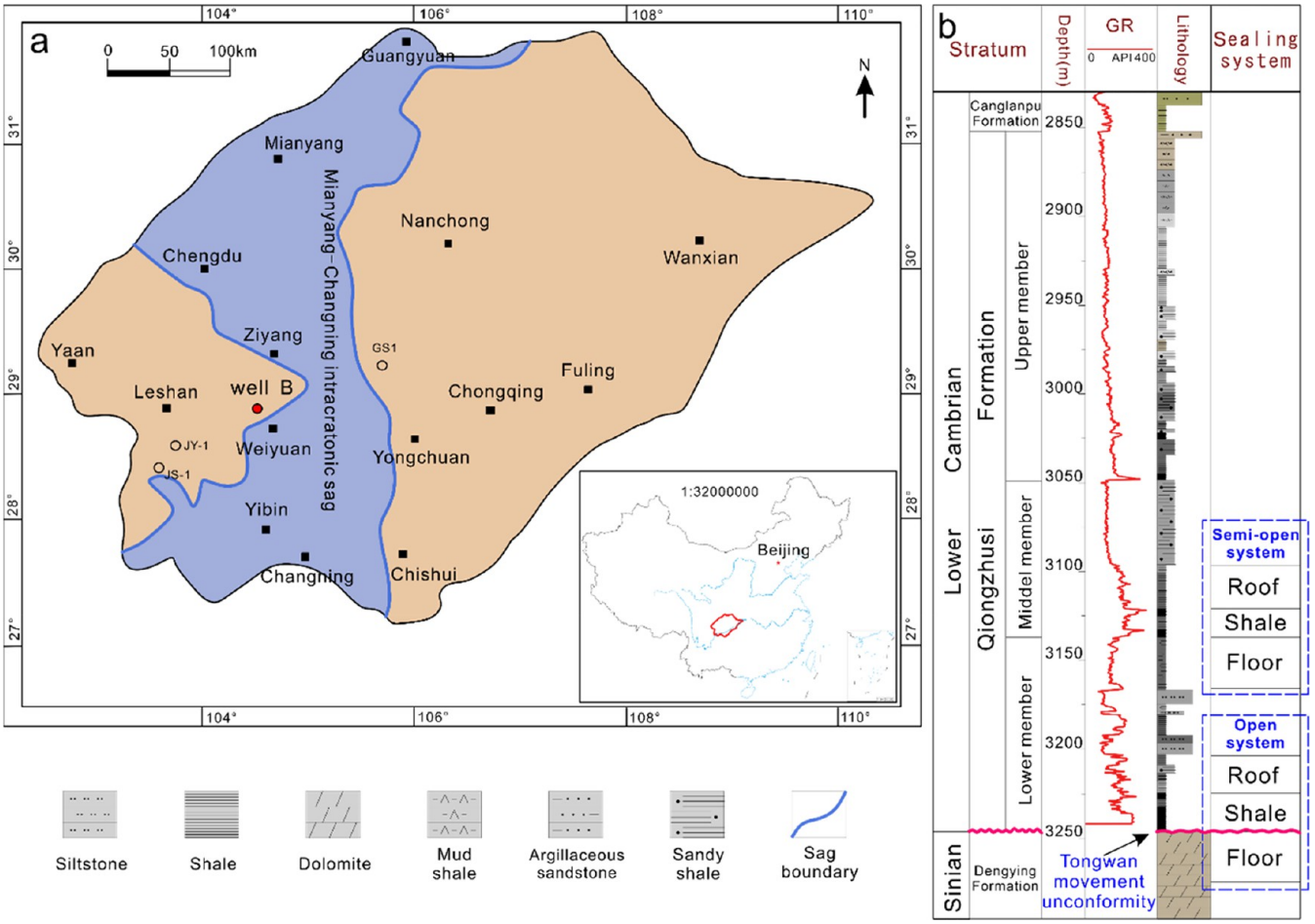


**Figure 1.** Location map and stratigraphic column of study well. (a) Schematic map showing the location of Well B and intracratonic sag (modified from Liu et al.[31]). (b) Stratum, GR, lithology, and sealing system of Well B.

pore formation, destruction, and preservation during the shale burial process.[13] Compaction leads to the rapid loss of primary large-sized pores in the early burial process.[14] The pores occupied by minerals (e.g., pyrite, carbonate, and phosphate) are formed during cementation. Tectonic deformation affects the development and distribution of different types of pores.[15−18] Moreover, the formation of OM pores is closely related to the cracking and conversion of OM during thermal maturation.[19−22] Acidic fluids released during the transformation of OM can dissolve chemically unstable minerals and form dissolution pores.[23] Furthermore, previous studies that have investigated the preservation conditions regarding faults, uplift, tectonic styles, and sealing capacity of the roof and floor have concluded that good preservation conditions are key factors and prerequisites for shale gas enrichment.[24,25] A rigid framework, pressure shadow, and overpressure play crucial roles in preserving pores,[23,26,27] implying that changes in minerals and pressure in shales affect the preservation condition. Because the Qiongzhusi Formation shale was formed early and experienced complex diagenesis during burial, the minerals and pores in the shale are strongly modified.[28] The roof and floor with evident differences control the sealing system of organic-rich shale, and the hydrocarbon expulsion behavior is distinctly dissimilar during thermal evolution.[6,29] More importantly, the hydrocarbon expulsion behavior influences the overpressure formation and shale gas enrichment.[30] Therefore, investigating the distribution and preservation of pores under different minerals and sealing systems can help understand the differences in the pores and gas content of the Qiongzhusi Formation.

In this study, the pore types and pore structures of the Qiongzhusi Formation shale were qualitatively and quantitatively characterized using field emission scanning electron microscopy (FE-SEM) and gas adsorption ($N_2$ and $CO_2$). Subsequently, the effects of minerals and sealing systems on shale pore preservation are discussed. Finally, the pore evolution patterns of different sealing systems of the Qiongzhusi Formation were established. This study will improve the understanding of the distribution and preservation of pore in shale and help assess the sweet-spot members for the Qiongzhusi Formation shale gas.

## 2. GEOLOGICAL SETTING

The Sichuan Basin, located in southwest China (Figure 1a), is a superimposed basin based on the Upper Yangtze Craton that undergoes multistage tectonic movements and has developed several regional unconformities.[31] In the late Sinian, the Sinian Dengying Formation dolomite was modified by different degrees of dissolution due to the Tongwan movement, resulting in good porosity and permeability. The regional unconformity between the Sinian and Cambrian is a reliable channel for hydrocarbon expulsion and migration (Figure 1b). The Weiyuan area is adjacent to the Mianyang-Changning intracratonic sag formed in the Early Cambrian (Figure 1a).


https://doi.org/10.1021/acsomega.2c00869
ACS Omega 2022, 7, 15821−15840

Table 1. Depth, TOC, and Mineral Composition of the Qiongzhusi Formation Shales for FE-SEM and Lower Pressure Absorption Experiments

| member | sample ID | depth (m) | TOC (%) | quartz (%) | reldspar (%) | total carbonate (%) | pyrite (%) | total clay (%) |
|---|---|---|---|---|---|---|---|---|
| upper member | U1 | 3000.59 | 0.49 | 34 | 19 | 9 | 3 | 35 |
| | U2 | 3021.79 | 0.94 | 37 | 13 | 9 | 3 | 38 |
| | U3 | 3025.67 | 1.03 | 32 | 12 | 12 | 3 | 41 |
| | U4 | 3043.95 | 2.06 | 33.8 | 14.5 | 13.2 | 3.5 | 35 |
| middle member | M1 | 3114.11 | 1.57 | 30 | 30 | 5 | 3 | 32 |
| | M2 | 3132.01 | 3.05 | 26 | 38 | 4 | 3 | 29 |
| lower member | L1 | 3151.99 | 1.33 | 38 | 27.1 | 13.9 | 3.9 | 17.1 |
| | L2 | 3177.64 | 0.24 | 36 | 32 | 14 | 1 | 17 |
| | L3 | 3229.28 | 2.41 | 38.4 | 20.9 | 6.5 | 10.9 | 23.3 |

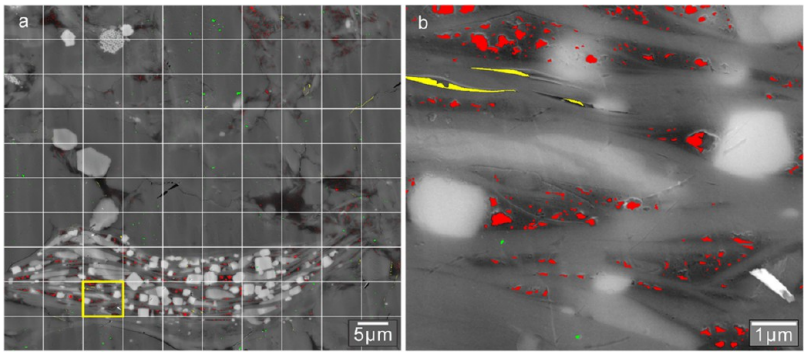


**Figure 2.** Example of quantitative analysis of different types of pores. (a) Stitched FE-SEM image (100 photos captured at 40000×). (b) Single FE-SEM image after quantitative analysis (red represents OM pore, green represents IntraP pore, and yellow represents InterP pore).

Owing to the subsidence of the Mianyang-Changning intracratonic sag and the rapid transgression, the Qiongzhusi Formation has compensatory deposition characterized by a large thickness of the Qiongzhusi Formation inside and small thickness outside the intracratonic sag.[31] The stratum thickness of the Qiongzhusi Formation in Well B of the Weiyuan area is approximately 400 m. The Qiongzhusi Formation can be divided into three members based on the core observations and logging data. In general, black shale, dark-gray shale, and dark-gray sandy shale dominated the middle and lower members of the Qiongzhusi Formation, whereas black shale, dark-gray argillaceous sandstone, and gray siltstone have developed in the upper member. Three sets of organic-rich shale were located at the bottom of each member.

## 3. SAMPLES AND METHODS

Nine shale samples from the Qiongzhusi Formation in Well B of the Weiyuan area were selected to be analyzed by the FE-SEM (Table 1). Argon ion polishing combined with FE-SEM has become an effective tool for shale pore structure studies (such as type, morphology, size, and number).[13,32] FE-SEM (Quanta 250 FEG, with EDS, INCAx-max20) and argon ion polishing (Gatan 697) experiments were performed at the State Key Laboratory of Oil and Gas Reservoir Geology and Exploitation, Chengdu University of Technology. All samples were mechanically cut and polished to obtain a flat surface for argon ion polishing. After argon ion polishing, the observed surface was sprayed with gold to enhance its electrical conductivity. Digital and quantitative processing of FE-SEM images has been used for quantitative analysis of shale pore structure.[33,34] In this study, FE-SEM quantitative analysis was performed using ImageJ software to obtain the pore parameters (e.g., Feret diameter, area, and perimeter) of different types of pores (Figure 2). Each image analyzed in Figure 5 comprises100 images captured at 40000× magnification.

Low-pressure adsorption ($N_2$ and $CO_2$) experiments were performed on nine samples at the same depth as the FE-SEM experiment (Table 1). The shale samples were crushed to 60−80 mesh and subsequently dried and degassed for 72 h. $N_2$ and $CO_2$ adsorption experiments were conducted at 77 and 273 K, respectively. Low-pressure adsorption experiments were performed at the Keyuan Engineering Technology Testing Center of Sichuan Province and were in accordance with the Chinese National Standard GB/T19587-2004. For $N_2$ adsorption data, the specific surface area and pore size distribution were interpreted using the Brunauer−Emmett−Teller and Barrett−Joyner−Halenda equations, respectively. For the $CO_2$ adsorption data, the specific surface area and pore size distribution were analyzed using density functional theory. In addition, fractal dimension was used to characterize the geometrical irregularities and roughness of the shale pores.[17,35] The fractal dimension can be calculated using the FHH model based on data obtained from $N_2$ adsorption.[36] The equations used are as follows

$$\ln(V/V_0) = K \ln[\ln(P_0/P)] + C \quad (1)$$

$$K = D - 3 \quad (2)$$

where $V$ is the volume of gas adsorption at equilibrium pressure $P$, $V_0$ is the monolayer coverage volume, $P_0$ is the saturation pressure, $P$ is the equilibrium pressure, $K$ is an exponent depending on the mechanism of adsorption and fractal dimension, $C$ is the constant of gas adsorption, and $D$ is the fractal dimension.

The sealing system of organic-rich shale is directly affected by the sealing capacity of the roof and floor. The lithology,



https://doi.org/10.1021/acsomega.2c00869
ACS Omega 2022, 7, 15821−15840

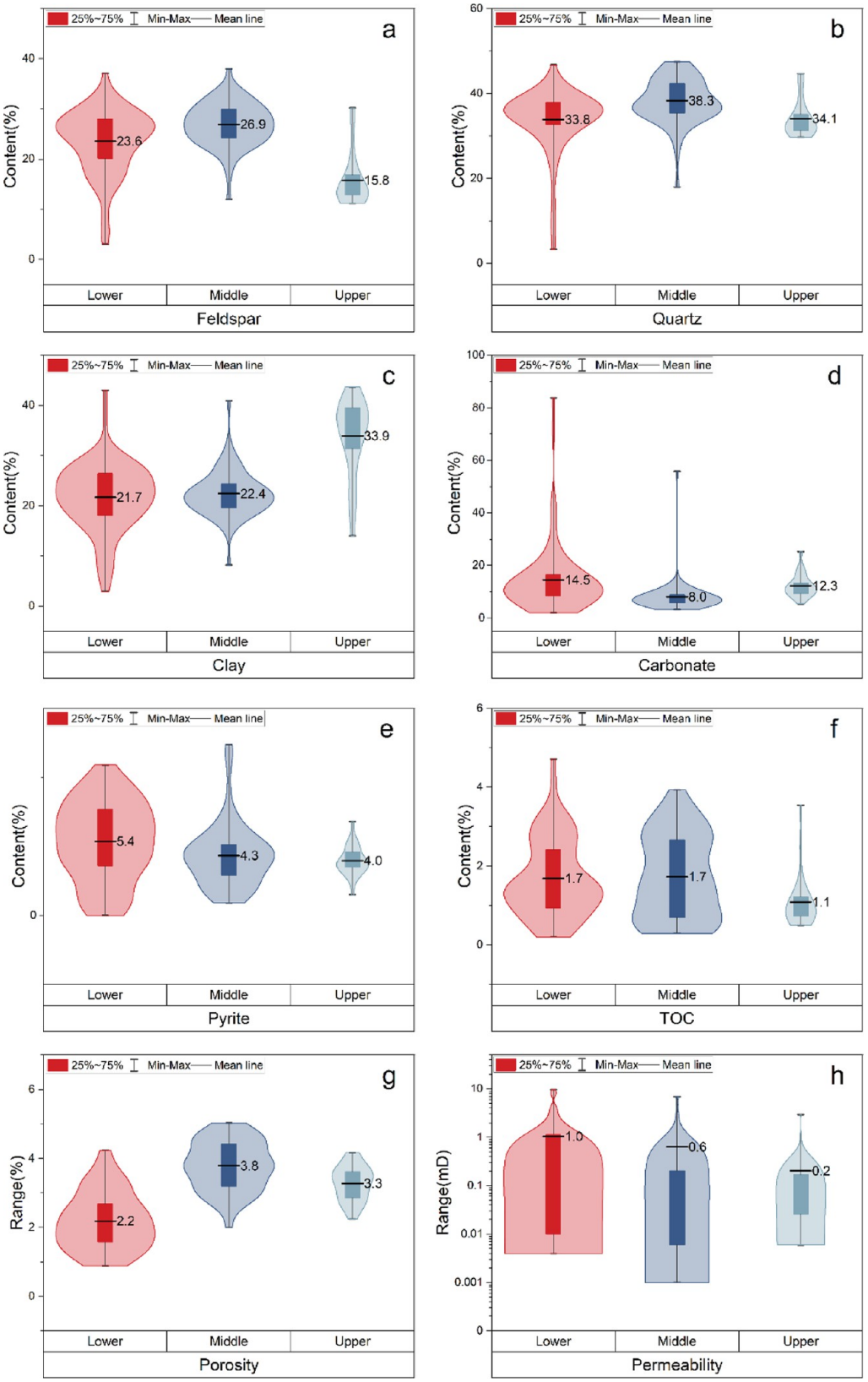


**Figure 3.** (a) Feldspar, (b) quartz, (c) clay, (d) carbonate, (e) pyrite, (f) TOC, (g) porosity, and (h) permeability of the Qiongzhusi Formation from the different members in Well B, Weiyuan Area.

thickness, porosity, permeability, breakthrough pressure, formation contact relationship, fault development characteristics, and gas content can effectively reflect the sealing capacity of the roof and floor.[29,37,38] In this study, the lithology, thickness, porosity, permeability, and formation contact relationship were used to evaluate the sealing capacities of the roof and floor of different sealing systems. In addition, data for 166 total organic carbon (TOC), 112 porosity, 172



https://doi.org/10.1021/acsomega.2c00869
ACS Omega 2022, 7, 15821−15840

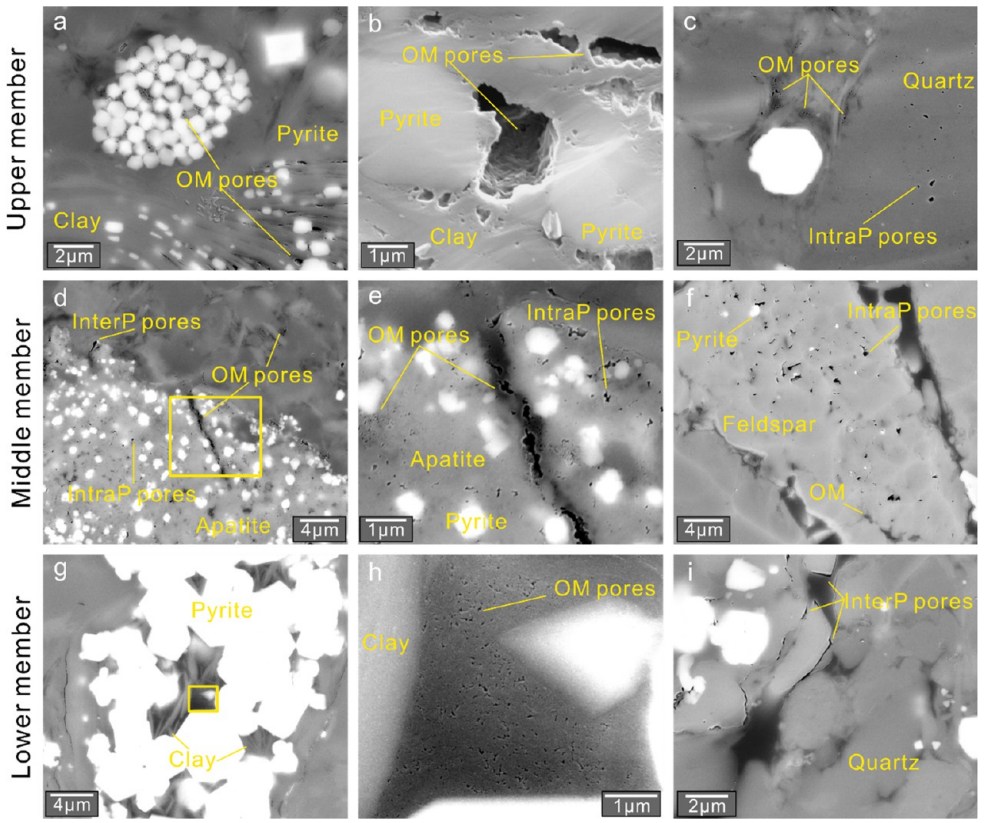


**Figure 4.** FE-SEM images of different members of the Qiongzhusi Formation. (a) OM pores are developed in pyrite framboid and clay, sample U2. (b) The large OM pore contains small OM pores, sample U2. (c) OM pores are developed between minerals, and IntraP pores are developed in quartz, sample U3. (d) OM pores and IntraP pores are distributed in OM−apatite aggregate, sample M2. (e) Magnified image of the yellow square in (d). (f) IntraP pores are distributed in feldspar. Some OMs and pyrites are developed in the IntraP pores, sample M2. (g) OM and clay are developed in pyrite framework, sample L3. (h) Magnified image of the yellow square in (g), OM pores are small and flat, sample L3. (i) InterP pores are distributed between minerals, sample L2.

**Table 2. Number, Diameter, and Relative Proportion of Surface Porosity for Different Types of Pores in Different Members of the Qiongzhusi Formation Shale**

| member | pore type | no. of pores | min diameter (nm) | max diameter (nm) | avg diameter (nm) | relative proportion of surface porosity (%) |
|---|---|---|---|---|---|---|
| upper member | OM pore | 7163 | 4 | 668 | 46.8 | 72.1 |
| | IntraP pore | 579 | 4 | 634 | 83.3 | 18.5 |
| | InterP pore | 220 | 4 | 1457 | 146.1 | 9.4 |
| middle member | OM pore | 4554 | 4 | 679 | 37.4 | 50.2 |
| | IntraP pore | 4081 | 4 | 263 | 39.3 | 46 |
| | InterP pore | 144 | 4 | 590 | 64.3 | 3.8 |
| lower member | OM pore | 6804 | 4 | 189 | 24.9 | 18.7 |
| | IntraP pore | 455 | 4 | 197 | 101.1 | 38.2 |
| | InterP pore | 880 | 4 | 3508 | 170.9 | 43.1 |

permeability, and 167 mineral compositions were collected from CNPC Chuanqing Drilling Engineering Company, Ltd.

## 4. RESULTS

**4.1. Mineralogy, TOC, Porosity, and Permeability.** Mineral component analysis indicated that quartz, feldspar, and clay are the main minerals of the Qiongzhusi Formation shales, with small amounts of carbonate minerals and pyrite (Table 1 and Figure 3a−e). The upper member of the Qiongzhusi Formation is mainly composed of quartz and clay minerals, whereas the middle and lower members are composed of quartz and feldspar (Figure 3). The TOC content of the Qiongzhusi Formation ranges between 0.2%−4.71%, with an average of 1.68%. Three sets of organic-rich (TOC > 2%) shales were developed in the Qiongzhusi Formation, located at the bottom of the upper, middle, and lower members. (Figure 1b). Generally, the TOC contents of the lower and middle members were higher than that of the upper member (Figure 3f). The total porosity of the Qiongzhusi Formation shale ranges from 0.88%−5.03%, with an average of 2.92%. However, the porosity of each member of the Qiongzhusi Formation was different. The lower member had the lowest porosity, the middle member had the highest porosity, and the upper member was between the two (Figure 3g). Moreover, the permeability of these shales ranged from 0.001−9.5987 mD, with an average of 0.7669 mD (Figure 3h).

**4.2. Pore Characteristics and Quantitative Analysis from FE-SEM Images.** According to the FE-SEM images



https://doi.org/10.1021/acsomega.2c00869
ACS Omega 2022, 7, 15821−15840

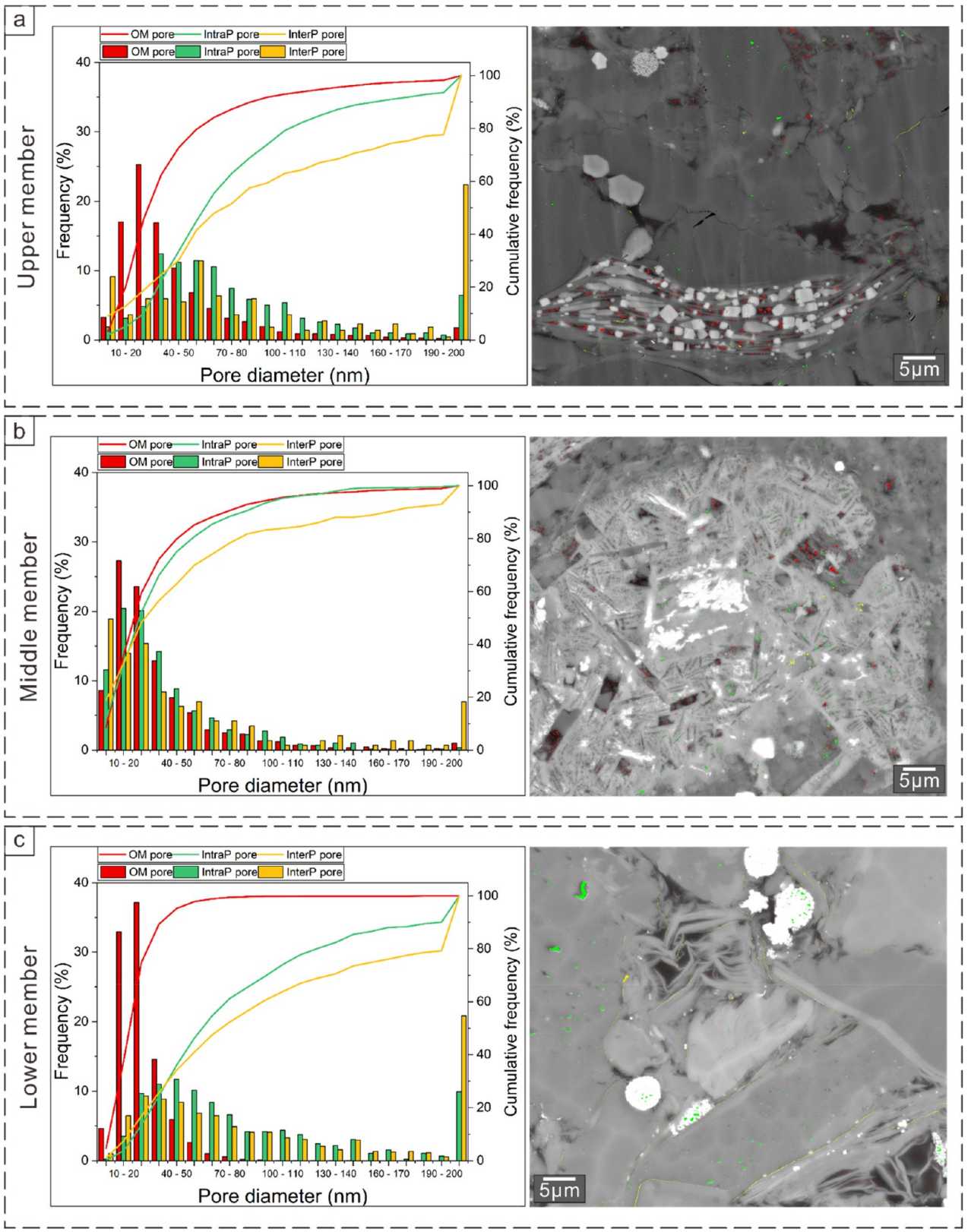


**Figure 5.** Pore size distribution of different types of pores in the Qiongzhusi Formation shale based on FE-SEM quantitative statistics. (a) Sample U3. (b) Sample M2. (c) Sample L3.

(Figure 4), the visible pores of the Qiongzhusi Formation shale were divided into OM pore, interparticle (InterP) pore, and intraparticle (IntraP) pore based on the pore classification proposed by Loucks et al.[13] The pore size distribution and pore structural parameters of the organic-rich shales in the three members are presented in Table 2 and Figure 5. The characteristics of the three pore types differed significantly for each member.



https://doi.org/10.1021/acsomega.2c00869
ACS Omega 2022, 7, 15821−15840

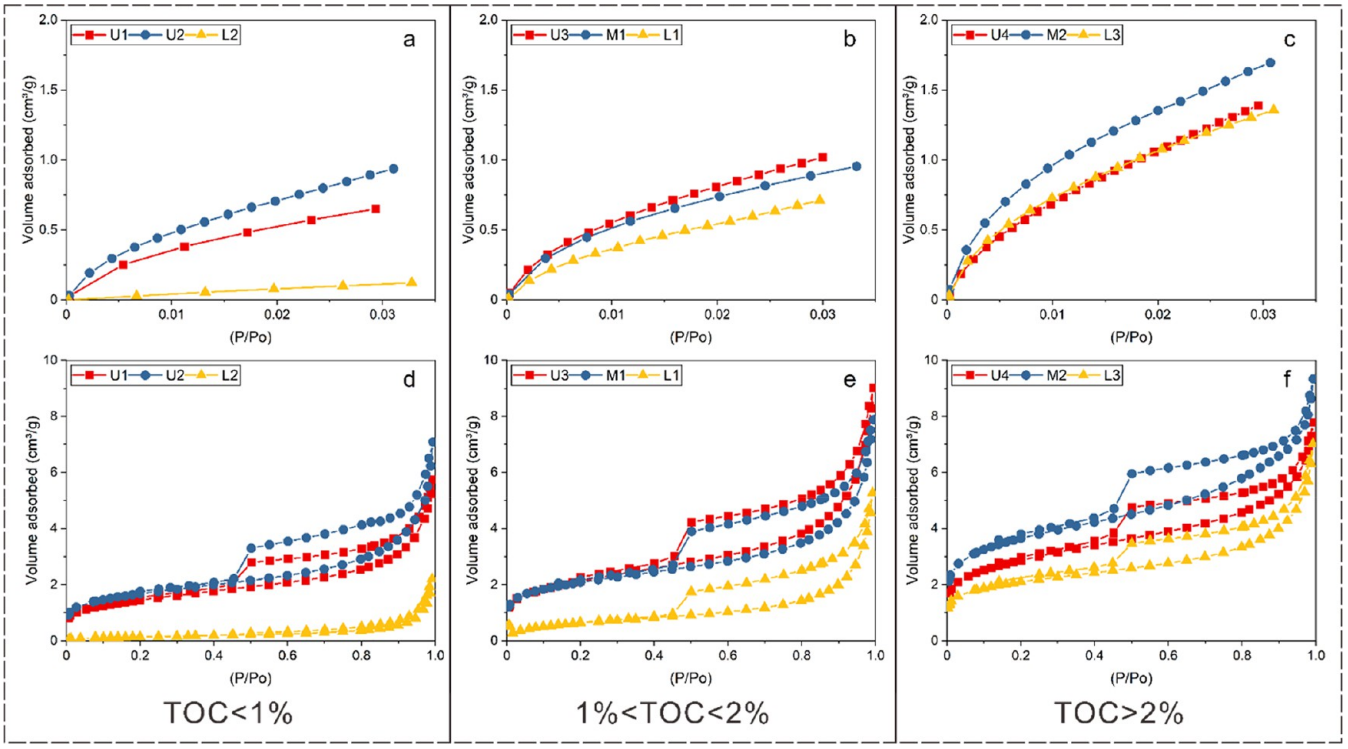


**Figure 6.** $CO_2$ and $N_2$ adsorption isotherms of the Qiongzhusi Formation shales with different TOC ranges. (a−c) $CO_2$ adsorption isotherms. (d−f) $N_2$ adsorption isotherms.

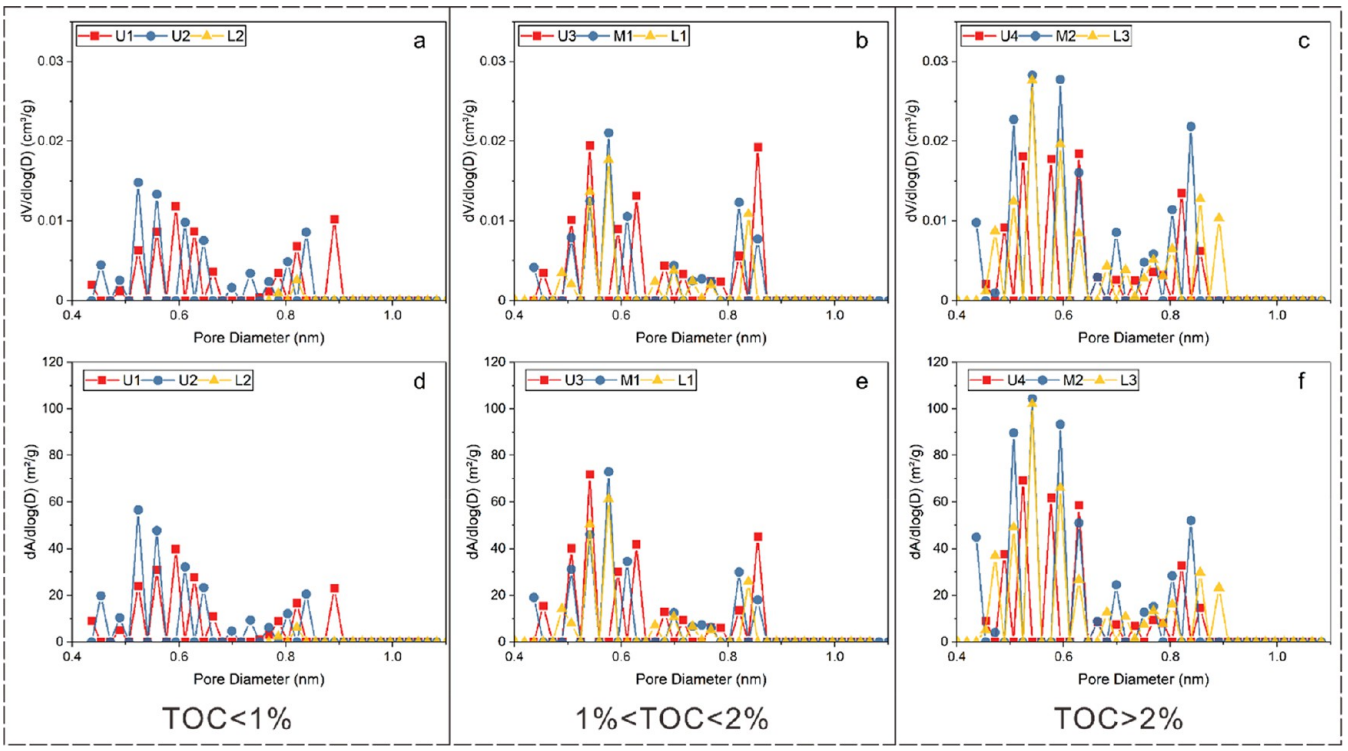


**Figure 7.** Log differential pore volume and specific surface area derive from $CO_2$ adsorption of the Qiongzhusi Formation shales with different TOC ranges. (a−c) $CO_2$ Log differential pore volume. (d−f) $CO_2$ Log differential specific surface area.

*4.2.1. OM Pores.* Most OM pores in each member of the Qiongzhusi Formation shale were identified within OM−clay, OM−apatite, OM−rutile aggregates, pyrite framboids, or rigid mineral particles (Figure 4). The morphology, number, and size of OM pores varied in each member of the Qiongzhusi Formation. Specifically, the OM pores in the upper- and middle-member shales are round, elliptical, and irregular (Figures 4b,d, and 10d). The morphology of these pores is characteristic of small pores fusing to form large pores. Additionally, smaller pores were observed within the rough



https://doi.org/10.1021/acsomega.2c00869
ACS Omega 2022, 7, 15821−15840

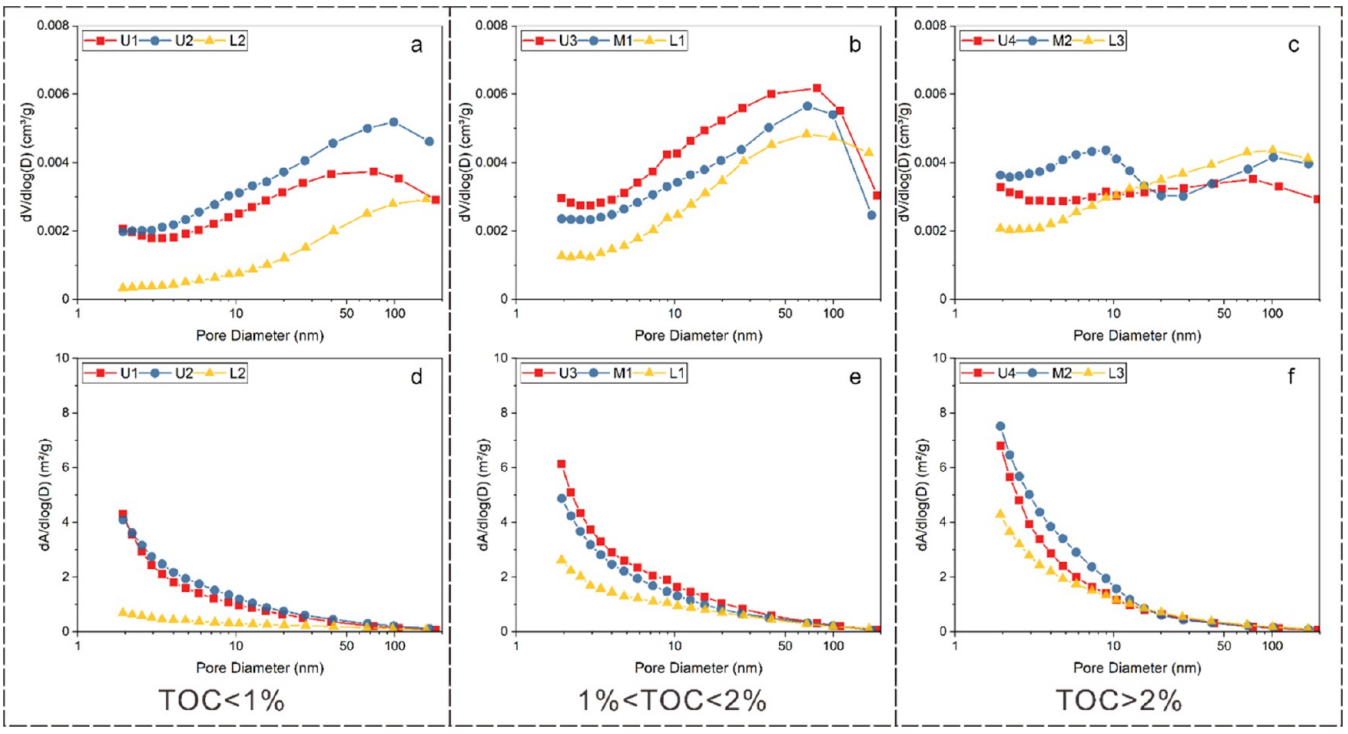


**Figure 8.** Log differential pore volume and specific surface area derive from $N_2$ adsorption of the Qiongzhusi Formation shales with different TOC ranges. (a−c) $N_2$ Log differential pore volume. (d−f) $N_2$ Log differential specific surface area.

inner walls of the larger pores (Figure 4b). In contrast, it was challenging to observe the OM pores of the lower member in the OM between the mineral particles (Figure 4i). Only a few tiny elliptical or slit-shaped OM pores were observed in some OM well protected by the mineral framework (Figure 4g,h). The diameter of the OM pores in the lower member shale was significantly smaller than that in the upper and middle member shales. The average diameter of OM pores in the lower member shale was narrowed by 46.8% and 33.5% compared to the upper and middle member shales, respectively. In addition, the relative proportion of surface porosity for OM pores in the lower member shale was also the lowest (Table 2).

*4.2.2. InterP Pores and IntraP Pores.* InterP pores were distributed among different minerals with triangular and irregular polygons (Figure 4i). IntraP pores were found within dissolution-related minerals, including quartz and feldspar (Figure 4c and f). The morphology of the IntraP pores was angular or irregular polygonal. Notably, in the middle member of the Qiongzhusi Formation, many IntraP pores were observed inside the OM−apatite aggregates and OM−rutile aggregates (Figures 4d,e and 13). The InterP pores and IntraP pores have a wide range of pore size distributions. Most inorganic pores were larger in diameter than OM pores (Table 2). Approximately 5−20% of inorganic pores had diameters greater than 200 nm (Figure 5).

**4.3. $CO_2$ and $N_2$ Adsorption.** Figure 6 shows the $CO_2$ and $N_2$ adsorption isotherms of different members of the Qiongzhusi Formation. All $CO_2$ isotherms were similar to Type I as classified by the International Union of Pure and Applied Chemistry (IUPAC) classification,[39] indicating the presence of micropores in the Qiongzhusi Formation shale. The maximum $CO_2$ adsorption quantity ranged from 0.12−1.69 $cm^3/g$, with an average of 0.98 $cm^3/g$. Most $N_2$ isotherms were similar to Type IV, except for sample L2 which contained an isotherm showing Type V. Notably, even when the maximum relative pressure was reached, no saturation adsorption plateau was observed in all isotherms, implying that the macropores in the samples were not saturated.[40] The hysteresis loops of all samples show a mixture of Type H2 and H3, suggesting that the pores of the Qiongzhusi Formation shale are ink-bottle-like and slitlike in shape. Notably, the maximum adsorption quantity and hysteresis loops of the samples in the lower member were smaller than those of the upper and middle members (Figure 6d−f).

The log differential pore volume and specific surface area curves for $CO_2$ adsorption showed similar trends (Figure 7). There were two stable peaks at approximately 0.4−0.7 and 0.8−0.9 nm, indicating that these pores contributed to the major pore volume and specific surface area. The contributions of micropores to the pore volume and specific surface area were positively related to the TOC content (Figure 15).

The log differential pore volume and specific surface area of $N_2$ revealed that most shale samples with TOC less than 2% displayed a prominent peak at a pore size of approximately 70−100 nm and a weak peak at 2−4 nm (Figure 8). For samples with TOC greater than 2%, the middle and upper shales exhibited more obvious bimodal characteristics than the lower shale. Furthermore, mesopores (especially those less than 10 nm) contributed to most of the specific surface area of the shale. Consequentially, the pore volume and specific surface area provided by mesopores (2−10 nm) in the lower member of the Qiongzhusi Formation were lower than those in the other members at each TOC content range.

**4.4. Fractal Dimension.** The plots of ln $V$ versus ln[ln($P_0$/$P$)] obtained from the original low-pressure $N_2$ adsorption data for the Qiongzhusi Formation shale are presented in Figure. 9. As shown by the $N_2$ adsorption and desorption curves (Figure 6d−f), the hysteresis loop of the curve appeared at $P/P_0$ =


https://doi.org/10.1021/acsomega.2c00869
ACS Omega 2022, 7, 15821−15840

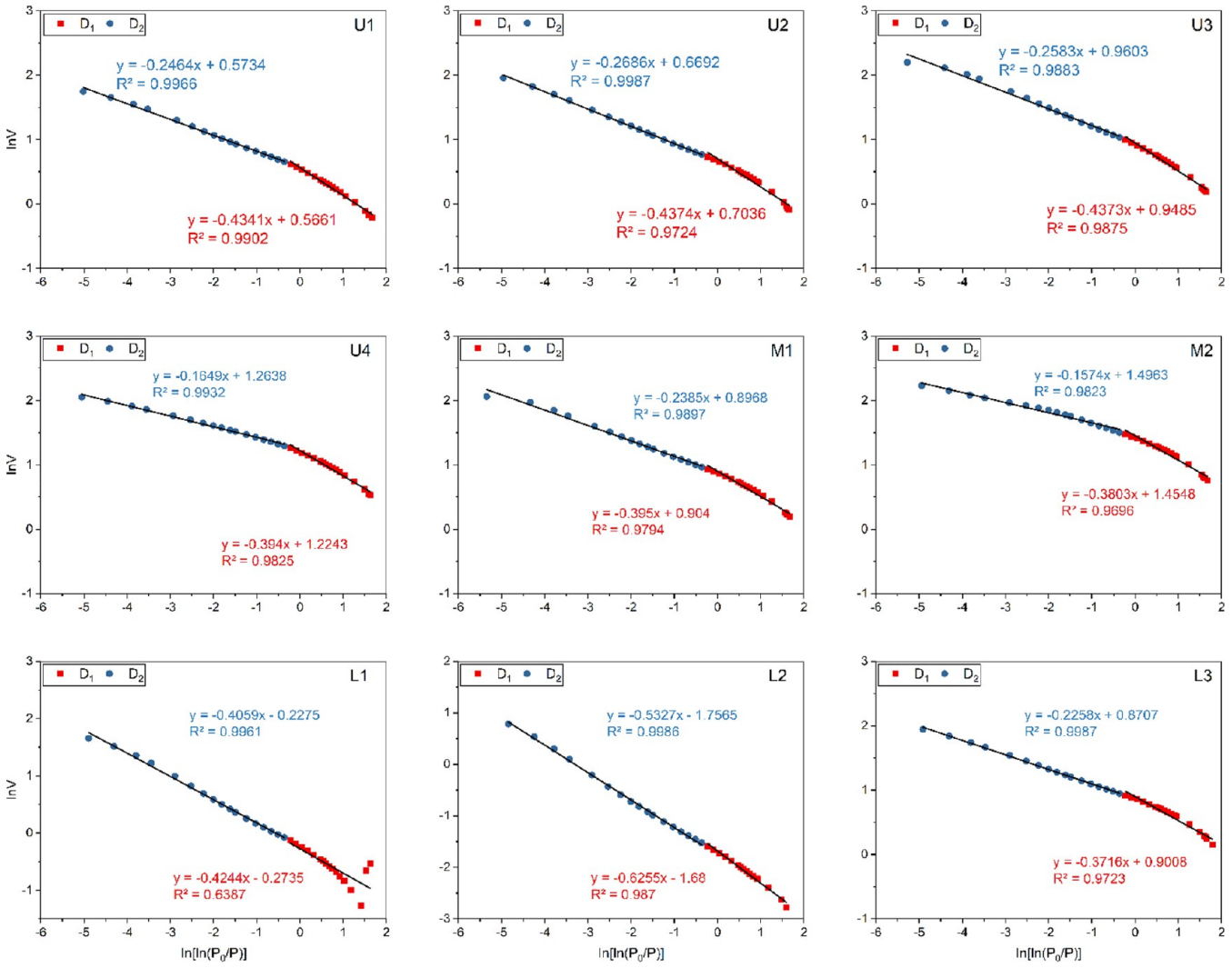


**Figure 9.** Fractal dimension calculation obtained from low-pressure $N_2$ adsorption data for the Qiongzhusi Formation shales

0.45, indicating that there were differences in the pore structure with different adsorption mechanisms in the two regions. Therefore, the fractal dimensions of the two regions were calculated separately. $D_1$ represents the fractal dimension of the relatively small pores in the low-pressure stage ($P/P_0$ < 0.45), whereas $D_2$ represents the fractal dimension of the relatively large pores in the high-pressure stage ($P/P_0$ > 0.45).

$D_2$ ranging from 2.4673 to 2.8426 (average = 2.7223) is larger than $D_1$ ranging from 2.3745 to 2.6284 (average = 2.5667), implying that the relatively large pores are more complex. The phenomenon of large OM pores containing small pores was observed using FE-SEM (Figure 4b); the results were consistent with the differences of fractal dimensions. In particular, the correlation coefficients of the linear fits for the $D_1$ fractal dimension of the L1 samples were low ($R^2$ = 0.6387), implying that fractal features may not be present in relatively small pores. Moreover, the fractal dimensions of the upper and middle members of the Qiongzhusi Formation shales are usually larger than those of the lower member shales in $D_2$ values (Table 3), suggesting that the pores in the middle and upper shales are more complicated.

**Table 3. Fractal Dimensions of the Qiongzhusi Formation Shales**

| | $P/P_0$: 0−0.45 | | | $P/P_0$: 0.45−1 | | |
|---|---|---|---|---|---|---|
| sample ID | $K_1$ | $D_1$ | $R^2$ | $K_2$ | $D_2$ | $R^2$ |
| U1 | 0.4341 | 2.5659 | 0.9902 | 0.2464 | 2.7536 | 0.9966 |
| U2 | 0.4374 | 2.5626 | 0.9724 | 0.2686 | 2.7314 | 0.9987 |
| L2 | 0.6255 | 2.3745 | 0.987 | 0.5327 | 2.4673 | 0.9986 |
| U3 | 0.4373 | 2.5627 | 0.9875 | 0.2583 | 2.7417 | 0.9883 |
| M1 | 0.395 | 2.605 | 0.9794 | 0.2385 | 2.7615 | 0.9897 |
| L1 | 0.4244 | 2.5756 | 0.6387 | 0.4059 | 2.5941 | 0.9961 |
| U4 | 0.394 | 2.606 | 0.9825 | 0.1649 | 2.8351 | 0.9932 |
| M2 | 0.3803 | 2.6197 | 0.9696 | 0.1574 | 2.8426 | 0.9823 |
| L3 | 0.3716 | 2.6284 | 0.9723 | 0.2258 | 2.7742 | 0.9987 |

## 5. DISCUSSION

**5.1. Response of Pore Characteristics of Shale to Minerals.** Previous studies have suggested that the support effect caused by rigid minerals protects the residual primary pores.[13,23,41] It is difficult to observe primary pores in the Qiongzhusi shale under strong compaction, but OM distributed among the rigid particles can be observed (Figure 10c). Meanwhile, the pressure shadow formed by the rigid minerals protects the OM pores in this organic matter (Figure



https://doi.org/10.1021/acsomega.2c00869
ACS Omega 2022, 7, 15821−15840

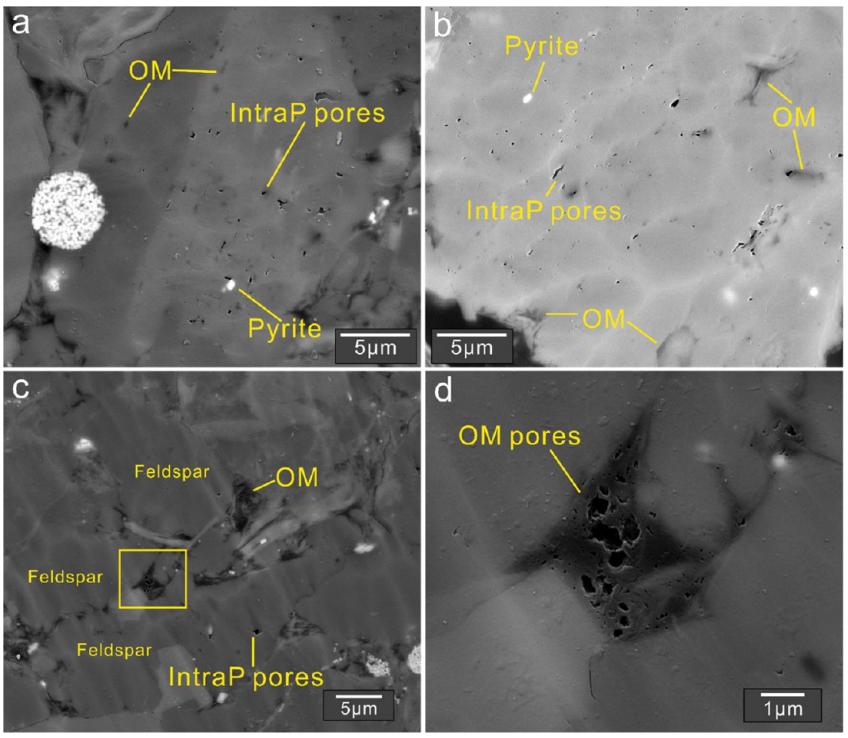


**Figure 10.** FE-SEM images of feldspars in the Qiongzhusi Formation. (a,b) IntraP pores are slit-like, elliptical, and varied in size. OM and pyrite were distributed in IntraP pores. (c) Organic matter is distributed between feldspars. (d) Magnified image of the yellow square in (c); IntraP pores are round and elliptical.

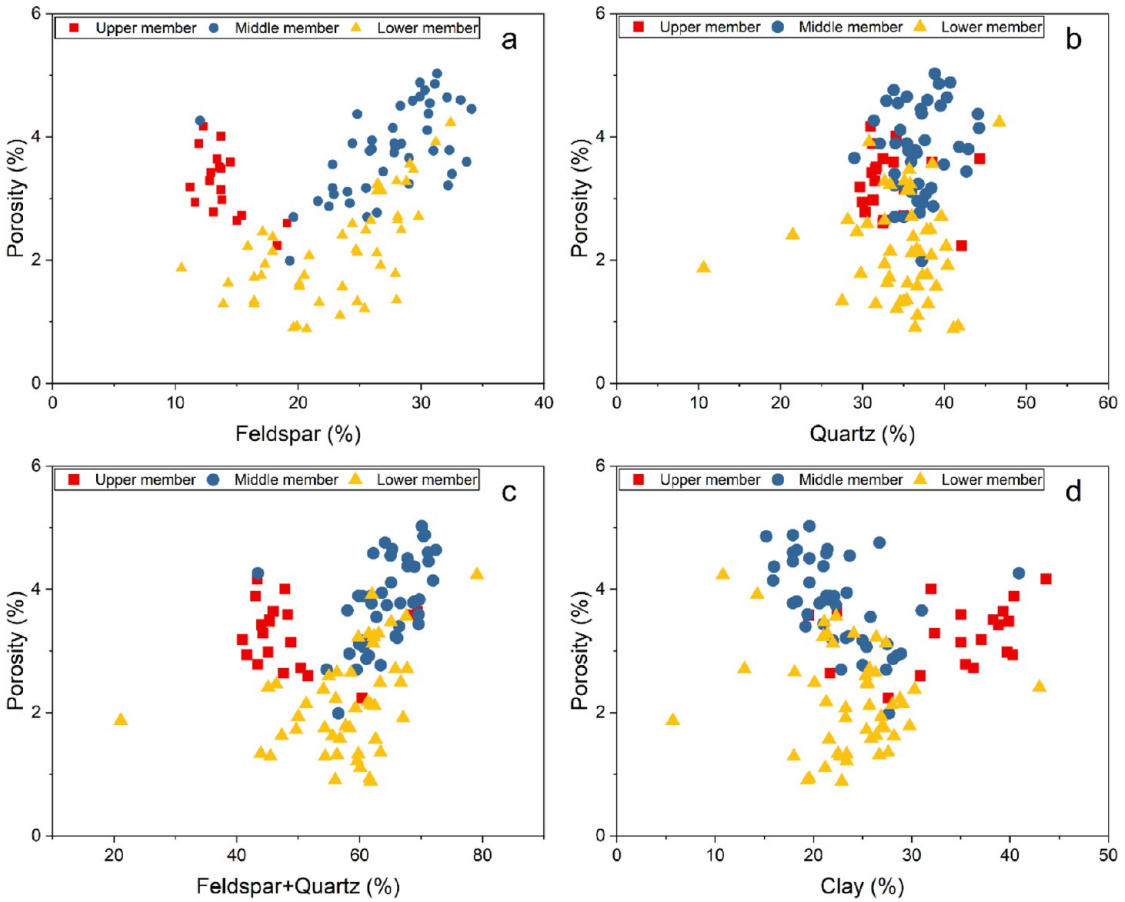


**Figure 11.** Correlation between porosity and (a) feldspar, (b) quartz, (c) feldspar and quartz, (d) clay of the Qiongzhusi Formation shales in different members.



https://doi.org/10.1021/acsomega.2c00869
ACS Omega 2022, 7, 15821−15840

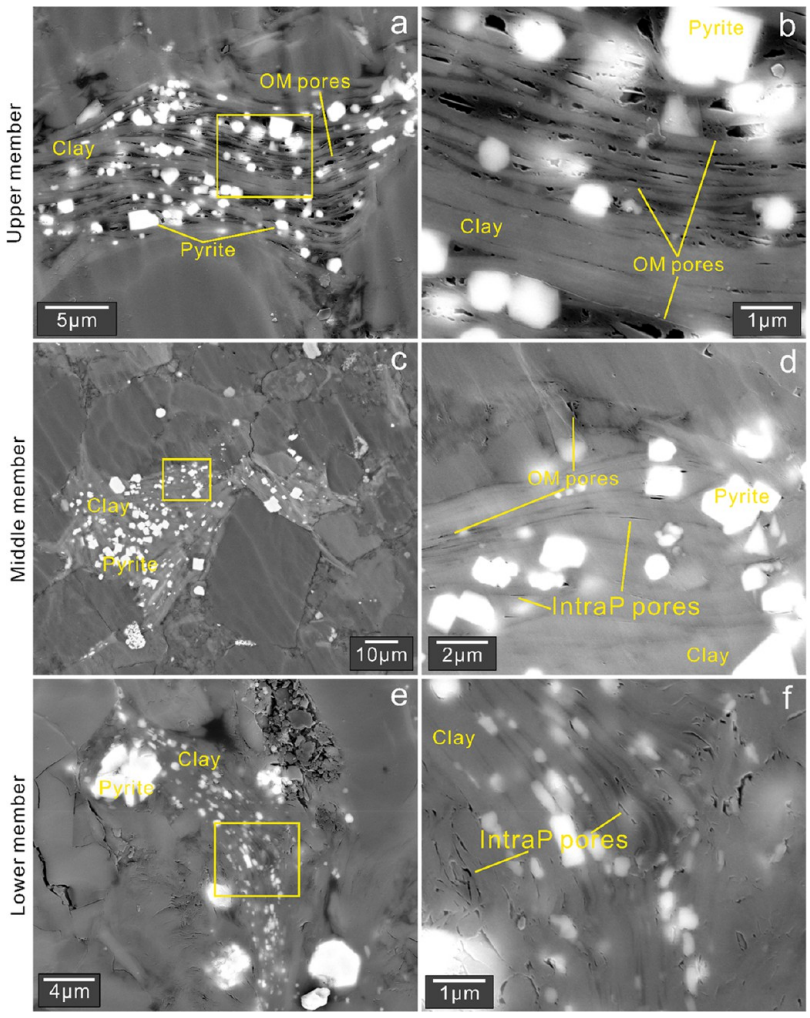


**Figure 12.** FE-SEM images of pores associated with clay in different members of the Qiongzhusi Formation. (a) Pyrites and organic matters fill in the deformed clay layer, sample U3. (b) Magnified image of the yellow square in (a); OM pores are elliptical. (c) Deformed clay in shale, sample M1. (d) Magnified image of the yellow square in (c); OM pores and IntraP pores are slitlike. (e) Deformed clay in shale, sample L3. (f) Magnified image of the yellow square in (e); IntraP pores are slitlike.

10d). According to previous studies, quartz content tended to be positively correlated with porosity or pore volume.[42,43] However, we discovered that there was no apparent correlation between quartz and porosity (Figure 11b), whereas feldspar showed a positive trend with the porosity of the Qiongzhusi shales (Figure 11a). The quartz content of the Qiongzhusi Formation was relatively stable, whereas the feldspar content is various (Figure 3a,b). The feldspar particles were large, often exceeding 25 $\mu$m, as observed in the FE-SEM images (Figure 10). Thus, the rigid framework and the pressure shadows may protect more pores associated with feldspar.

It is worth noting that feldspar is richer in IntraP pores than quartz in the Qiongzhusi Formation shale (Figure 4c,f). IntraP pores in quartz are often considered isolated and do not contribute significantly to the porosity and permeability.[42] However, some IntraP pores in feldspar were filled with organic matter and pyrite (Figure 10a,b), indicating that IntraP pores in feldspar are not isolated but are connected to the Qiongzhusi shale matrix. Feldspar is a chemically unstable mineral that is dissolved by organic acids that are released during the thermal maturation of OM and form IntraP pores.[23] Additionally, the pores in some feldspars may be related to the albitization of K-feldspar. Min et al.[44] observed the albitization of K-feldspar in the Qiongzhusi Formation shale and suggested that feldspar shrank in bulk and formed new pores, which were often filled with OM, clay, and pyrite during the diagenetic process. Compared to OM, siliceous minerals often cannot adsorb methane,[11] but IntraP pores modified by OM in feldspar might provide adequate adsorption space for shale gas.

Clay minerals and OM have strong physical and chemical activities, and they often appear in shale in the form of OM−clay aggregate.[45,46] In the Qiongzhusi shale, OM and pyrite particles are often distributed in the clay interlayer (Figure 12). Although most of the OM−clay aggregates were deformed by compaction (Figure 12a, c, and e), the rigid pyrite formed a pressure shadow structure between the clay mineral layers (Figure 12b), protecting the internal pores and organic matter.[27,47] However, the supporting effect of the rigid framework may be limited. There are evident differences in the OM content and pore development characteristics in the OM−clay aggregates of different members of the Qiongzhusi Formation (Figures 11d and 12). Specifically, OM distributed in clay minerals of the middle and lower members of the Qiongzhusi Formation is less than that in the upper member. Meanwhile, it is difficult to observe pores in the clay minerals of the lower member by comparing the FE-SEM images of clay


https://doi.org/10.1021/acsomega.2c00869
ACS Omega 2022, 7, 15821−15840

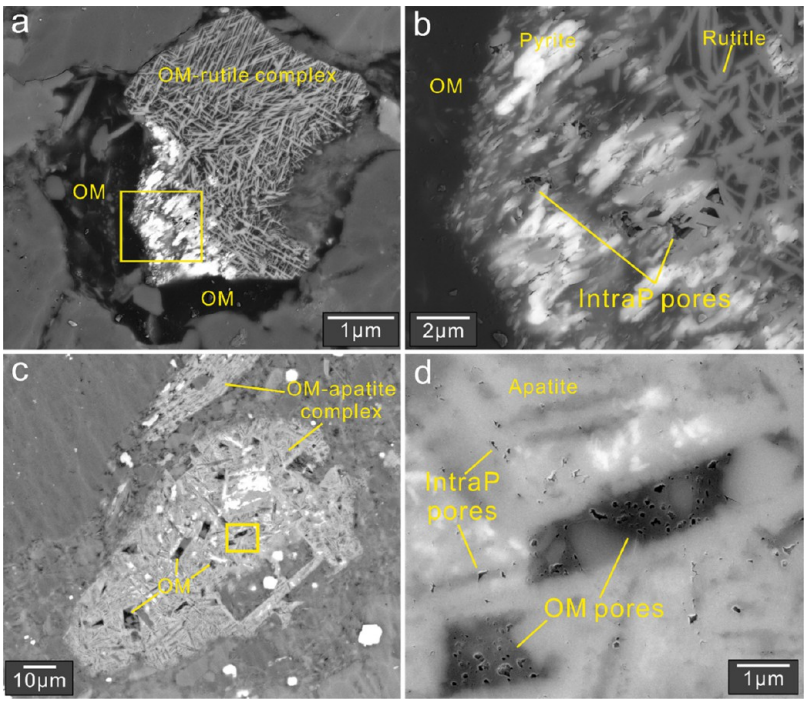


**Figure 13.** FE-SEM images of pores associated with OM−rutile and OM−apatite aggregates in different members of the Qiongzhusi Formation. (a) OM−rutile aggregate develops in sample M2. The rutile is arranged in a triangular shape. (b) Magnified image of the yellow square in (a); OM and IntraP pores are developed in the OM−rutile aggregate. (c) OM−apatite aggregate develops in sample M2. The apatite is arranged in a quadrilateral shape. (d) Magnified image of the yellow square in (c); OM pores are round and elliptical.

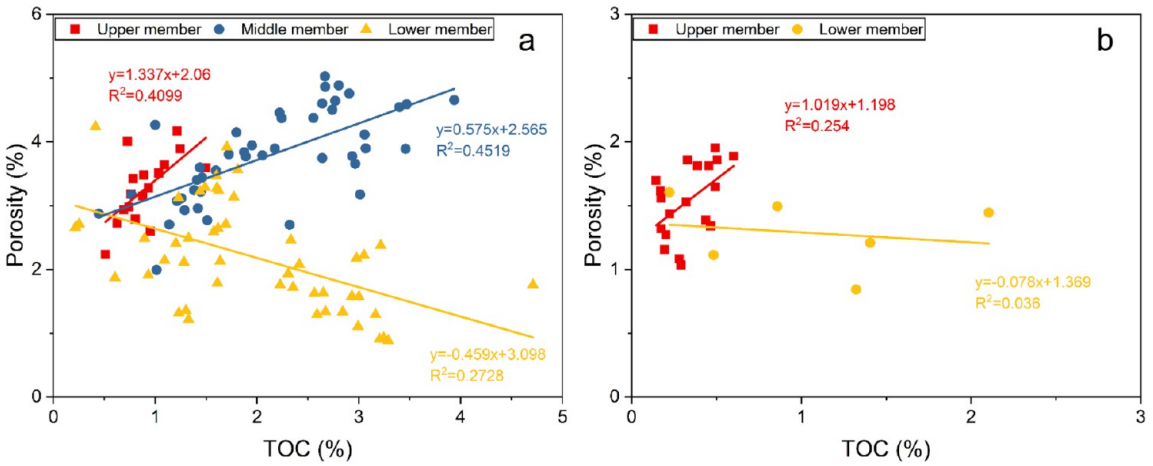


**Figure 14.** Correlation between TOC and porosity of the Qiongzhusi Formation in (a) Well B (data from this paper) and (b) in JY1 (data are adopted from Xiong et al.[52]).

minerals in different members of the Qiongzhusi Formation. The few visible pores were small and flat (Figures 4h and 12f). Kulia et al.[48] conducted compaction experiments on clay minerals and found that the pore volume of mesopores and macropores appeared to be significantly reduced with increasing pressure, whereas micropores were almost unaffected. Milliken et al.[49] suggested that intense compaction may cause OM to migrate into InterP pores. Under strong compaction, the pressure shadow structure of the OM−clay aggregate in the middle and lower members of the Qiongzhusi Formation may no longer have a protective effect against compaction. Some of the organic matter in the clay interlayer was discharged, and the OM pores disappeared.

OM−rutile and OM−apatite aggregates are observed in the middle member of the Qiongzhusi Formation shale (Figure 13). FE-SEM quantitative statistics showed that IntraP pores and OM pores contributed to the major surface porosity of the OM−apatite aggregate (Figure 5b). Ko et al.[50] observed preoil bitumen filled in the IntraP pores of phosphatic at the peak bitumen generation stage, implying that interconnected pore networks were developed within the phosphate. Unlike the randomly distributed rigid particles in the OM−clay aggregates, the minerals inside the OM−rutile and OM−apatite aggregates are often arranged in triangular or quadrilateral shapes (Figure 13b,d). The OM and pores were well protected in the more stable rigid frameworks. Differences in the type, characteristics, and distribution of pores in


https://doi.org/10.1021/acsomega.2c00869
ACS Omega 2022, 7, 15821−15840

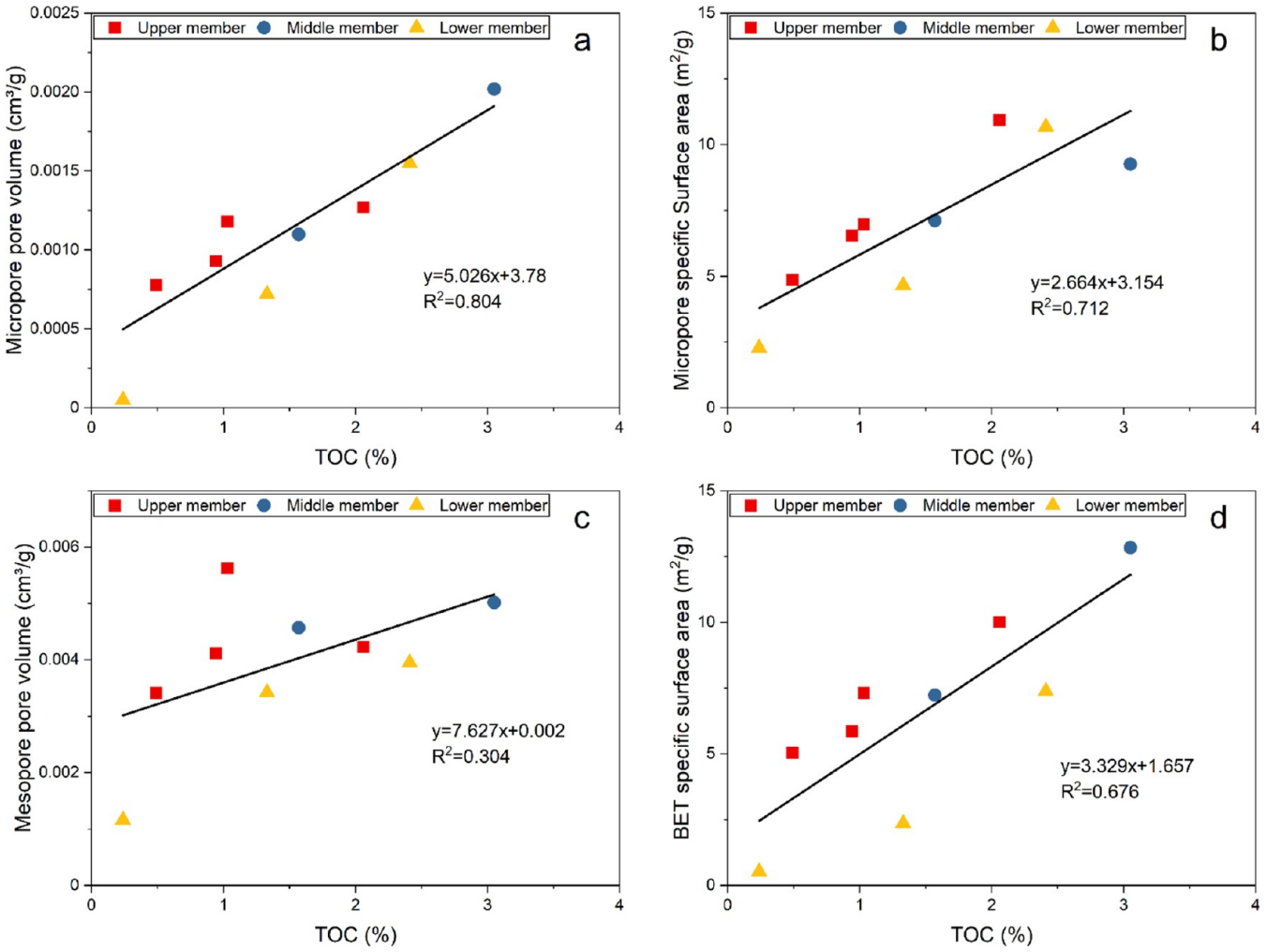


**Figure 15.** Correlation between TOC and (a) micropore pore volume, (b) pore structure parameters, (c) mesopore pore volume, and (d) BET specific surface area of the Qiongzhusi Formation shales.

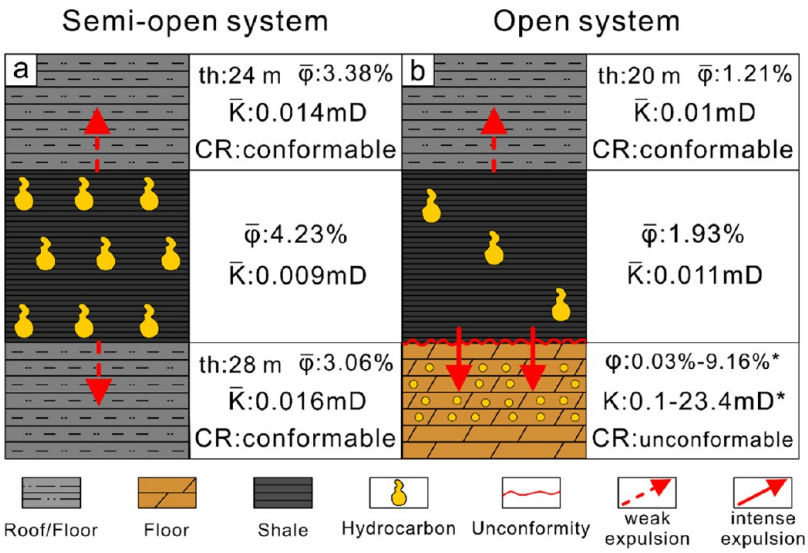


**Figure 16.** Comparison of the sealing parameters of (a) semiopen system and (b) open system. th: thickness, $\bar{\varphi}$: average porosity, $\bar{k}$: average permeability, CR: contact relationship, *: data from Sun et al.[62]

different minerals and aggregates are controlled by their physicochemical properties, combinations, and arrangements. Xu et al.[51] believed that changes in lithofacies affect the relative proportions of micropores, mesopores, and macropores under stable conditions of tectonic movement. In this study, OM pores tended to be distributed in multiple OM−mineral



https://doi.org/10.1021/acsomega.2c00869
ACS Omega 2022, 7, 15821−15840

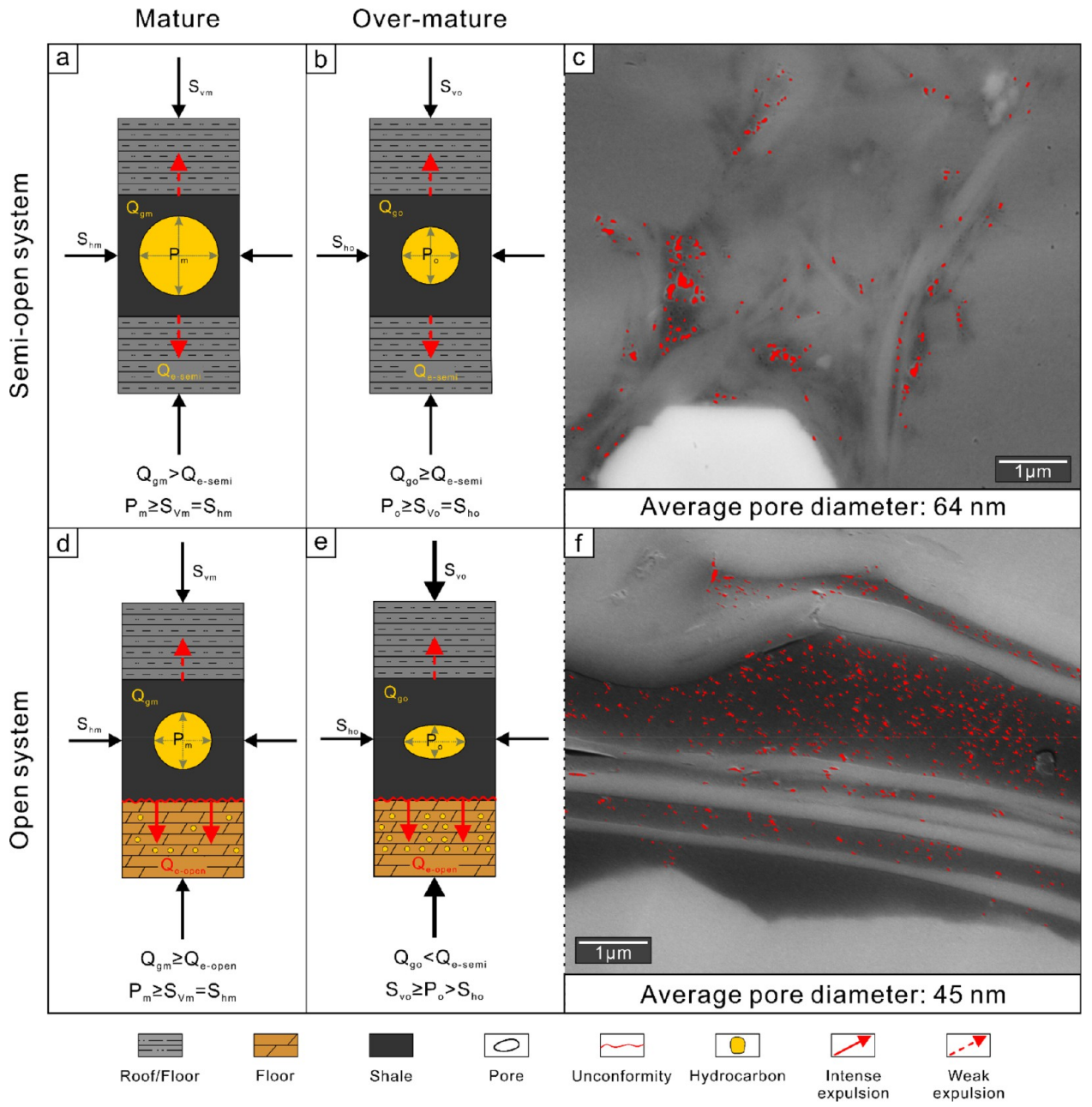


**Figure 17.** Schematic diagram of OM pore development characteristics in different sealing systems. (a,b) Variation of OM pores in the semiopen system. (c) OM pores extraction of sample M2. (d,e) Variation of OM pores in the open system. (f) OM pores extraction of sample L3.

aggregates and the organic matter with pressure shadow protection, and the inorganic pores were associated with feldspar, OM−apatite, and OM−rutile aggregates (Table 2 and Figure 5).

**5.2. Response of Pore Characteristics of Shale to Sealing Systems.** The porosity of different members of shales is significantly different in this study (Figure 3g). The correlation between TOC content and porosity exhibits two distinct trends (Figure 14a). Porosity is positively correlated with TOC content in the upper and middle member shales, implying that OM pores contribute to porosity. Conversely, there was a negative correlation between TOC and porosity in the lower member. A similar trend occurred in the Qiongzhusi Formation shales in the adjacent Well JY1 within the Sichuan Basin (Figure 14b),[52] implying that the difference might have occurred in the southern Sichuan Basin. This difference is also supported by the FE-SEM images (Figure 4b,e,h) and the quantitative analysis of OM pores (Figure 5), suggesting that the contribution of OM pores to porosity is significantly different among the various members of the Qiongzhusi Formation.

Figure 15 presents the correlation between the TOC and pore structure parameters to clarify the differences in microscopic OM pores. The micropore volume and specific surface area showed positive correlations with TOC content, consistent with the results of the Lower Cambrian and Lower Silurian Longmaxi Formation shales,[53,54] indicating that OM is the predominant controlling factor for micropores. However, weaker correlations were found between mesopore volume, specific surface area, and TOC (Figure 15c,d). Other studies have also reported a similar phenomenon of a stronger correlation between micropores and a weaker correlation



https://doi.org/10.1021/acsomega.2c00869
ACS Omega 2022, 7, 15821−15840

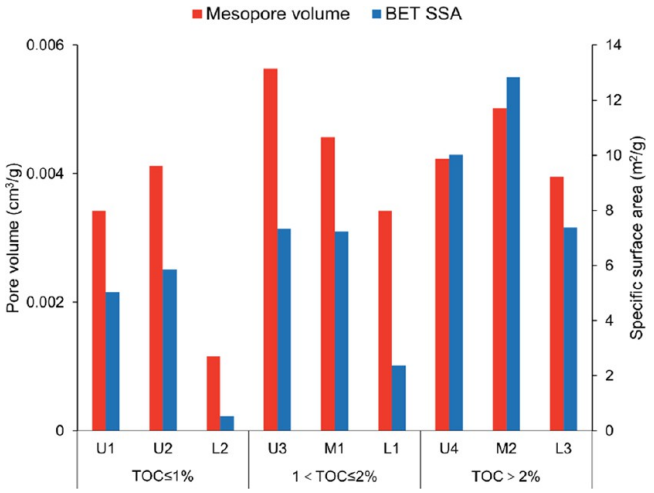


**Figure 18.** Mesopore volume and BET specific surface area of different members shale.

between mesopores.[53,55] In addition, fractal dimension $D_2$ is prominently different from the $D_1$ (Table 3), implying that the OM pores within the mesopore range might be strongly modified, whereas OM pores within micropores have little response.

Compaction or tectonic movements often causes modification of OM pores.[18,56] Milliken et al.[26] found that TOC content is positively correlated with porosity when TOC content is less than 5.5%, while porosity hardly increases with TOC when it is content greater than 5.5%, and visible pore face porosity decreases with increasing TOC content. The study concluded that the low-TOC samples have the support of the rigid mineral framework to avoid the pores being compacted. The mechanical properties of OM are significantly different from those of other minerals in shale.[57] An increased TOC content results in a decreased Young's modulus, thereby increasing the ductility of the shale,[58,59] which makes the shale and pores more likely to be compacted. Moreover, Ma et al.[16] suggested that compared to the non-deformed zone, OM pores in the mesopores and macropores in the deformed zone collapse during tectonic deformation.

However, the Qiongzhusi Formation shales in the middle and lower members had similar mineral compositions and organic geochemical characteristics (Figure 3). In particular, most TOC contents were within a similar range and did not exceed the turning point proposed by the previous study,[26] implying that the mechanical properties of the middle and lower members of the Qiongzhusi Formation were similar. Additionally, Well B is located in the Sichuan Basin, where the intensity of tectonic movements is generally lower than in the outer basin.[31] The burial history curve of Well GS1, which is close to that of Well B, reveals that the Qiongzhusi Formation began to be buried rapidly from the Triassic and changed to rapid uplift in the Late Cretaceous.[60] Hence, different member shales in the Qiongzhusi Formation for Well B underwent similar thermal and structural evolution processes.

The roof, floor, and organic-rich shale with different properties constitute sealing systems with different preservation conditions.[29,38,61] Good preservation conditions are significant for maintaining overpressure, pore preservation, and shale gas enrichment.[24,25] Therefore, the sealing systems of the Qiongzhusi Formation shale in the different members are quite different. Specifically, the middle and upper shales were semiopen systems. The organic-rich shale is conformably in contact with tight, low-porosity, and low-permeability roof and floor, and the thicknesses of the roof and floor were 24 and 28 m, respectively (Figure 16a). In contrast, the lower member of the Qiongzhusi Formation is an open system. Although the roof of the organic-rich shale in the lower member shale was 20 m thick and had a good sealing capacity, the sealing capacity of the floor was poor (Figure 16b). The strata of the Upper Yangtze Platform were uplifted and denuded by the Tongwan movement during the late Sinian.[31] Dissolution pores and fractures developed in the dolomite of the Dengying Formation under the influence of dissolution. Therefore, the Dengying Formation has high porosity and permeability and is a good reservoir with good physical properties and connectivity for oil and gas.[62] Additionally, a regional unconformity between the Sinian Dengying Formation and the Lower Cambrian Qiongzhusi Formation formed by the Tongwan movement becomes a window for the expulsion of hydrocarbons and a channel for migration from the organic-rich shales.[6] The homogenization temperature of the oil and gas inclusions in the Dengying Formation of the Well GS1 ranges from 90−240 °C. As the homogeneous temperature of inclusions increases, these inclusions gradually change from oil inclusions to gas inclusions.[60] This is consistent with the thermal evolution of the organic-rich shale of the Qiongzhusi Formation, implying that the Qiongzhusi Formation continuously expelled hydrocarbons during the burial process.

Under normal stratigraphic conditions, the rock skeleton bore overlying formation pressure. The mechanical properties and ability to resist compaction of the shale do not strongly differ when the mineral composition and OM content are similar.[57,58,63] However, cracking and converting OM causes volume expansion and overpressure generation while increasing thermal maturity.[64,65] Thermal simulation experiments under formation conditions suggested that the highest volume of gas produced during thermal evolution was 1720 times the volume of oil.[66] When the retention coefficient was 0.9, the maximum pressure coefficient of the Qiongzhusi Formation was 2.45.[67] When overpressure is present, the overlying formation pressure on organic-rich shale is borne by the shale mineral framework and the pore fluid. During the thermal evolution, the quantity of hydrocarbon generation ($Q_g$) controlled by OM decomposition and the quantity of hydrocarbon expulsion ($Q_e$) controlled by the sealing system affect the pore pressure variation in different sealing systems. Therefore, the stress equilibrium state between the pore pressure and external stress influences the shale compaction intensity.

Organic-rich shale has a strong hydrocarbon generation capacity in the mature stage. In the semiopen system of the Qiongzhusi Formation, the roof and floor with strong sealing capacity trap the hydrocarbons inside the organic-rich shale to form overpressure. The high pore pressure of the OM pores can resist the influence of horizontal and vertical stresses (Figure 17a). Consequently, the OM pores were large and round. In contrast, in the open system of the Qiongzhusi Formation, some of the hydrocarbons generated from organic-rich shales during thermal maturation can conveniently migrate through the unconformity and be stored in the Dengying Formation (Figure 16b). Liu et al.[67] suggested that overpressure is formed when the retention coefficient of the Qiongzhusi Formation shale is greater than 0.5. When the retention coefficient increased by 0.05, the pressure coefficient


https://doi.org/10.1021/acsomega.2c00869
ACS Omega 2022, 7, 15821−15840

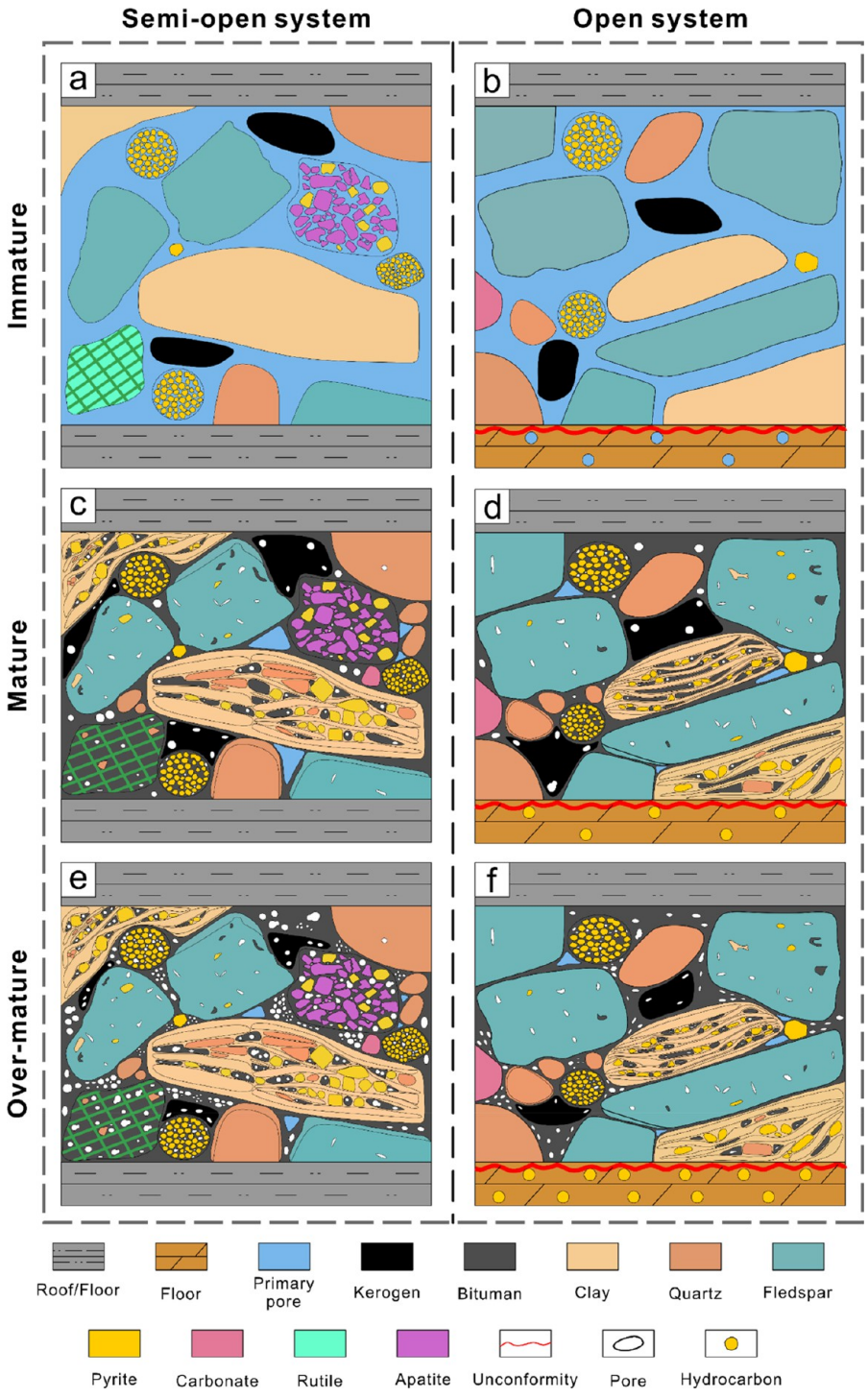


**Figure 19.** Generalized model for the evolution of OM and mineral pores of the Qiongzhusi Formation in the (a,c,e) semiopen system and (b,d,f) open system. different sealing systems.

increased by 0.3−0.4 at the same burial depth. Hence, the expulsion of hydrocarbons limits the increase in pore pressure. The size of the OM pore was reduced to maintain the stress equilibrium state between pore pressure and horizontal and vertical stresses (Figure 17d). In the overmature stage, the hydrocarbon generation capacity of the organic-rich shale gradually decreased. The pore size and morphology continuously changed with the variation of the stress equilibrium state in both the semiopen and open systems (Figure 17b,c;e,f). The pore pressure in the open system decreased more rapidly because of the poor sealing capacity and high hydrocarbon expulsion efficiency. Once the stress equilibrium state between the pore pressure and external stresses is disrupted, OM pores are deformed, narrowed, or even closed under the influence of compaction owing to the loss of overpressure support.

In this study, the pore pressure decreased more rapidly during burial because of the long hydrocarbon expulsion and high expulsion efficiency in the open system. Without overpressure protection, the OM pores in the open system are deformed more intensely than those in the semiopen


https://doi.org/10.1021/acsomega.2c00869
ACS Omega 2022, 7, 15821−15840

system. Therefore, OM pores in the open system are rare and flat or slitlike in shape (Figures 4h and 17c), while OM pores in the semiopen system are abundant and round or elliptical (Figures 4b and 17f). Meanwhile, the average diameter of the OM pores in the open system was the lowest, approximately 40.2% lower than that of the semiopen system (Table 2). Moreover, the pore volume and specific surface area of the mesopores for the shales in the open system were reduced by an average of 38.4% and 37.7%, respectively, compared to those in the semiopen system (Figure 18). The fractal dimensions $D_2$ of the semiopen systems were usually larger than those of the open systems (Table 3), implying that the pores in the middle and upper member shales are more complicated. Owing to the above differences, there are dissimilar trends in the correlation between porosity and TOC content (Figure 14).

When uplift and denudation affected the preservation conditions of shale, the thermal evolution of shale might have stopped. In contrast, sealing systems affect preservation conditions through the evolution of organic-rich shale, implying that fewer hydrocarbons remain in the shale. More importantly, the pores were intensively compacted without overpressure protection in an open system. The decrease in pore volume and specific surface area may further reduce the quantity of free gas and adsorbed gas in the shale.

**5.3. Conceptual Model of Pore Evolution for Different Sealing Systems.** Based on the analysis of the mineral composition, geochemical characteristics, pore characteristics, sealing systems, and pore evolution of the Qiongzhusi Formation shale,[13,50,64,68] we depicted the idealized models of the Qiongzhusi Formation shales during burial, expecting to deepen insight into the response of pore development characteristics to minerals and sealing systems.

The shale buries at a shallow depth in the early deposition stage and is not mature. Various minerals and OM are scattered within the shale, and the main pore space is dominated by primary pores (Figure 19a,b). As the burial evolution proceeds, compaction and cementation cause most of the primary pores to disappear.[14] Some primary pores are preserved under the rigid framework composed of rigid minerals such as feldspar, quartz, and pyrite.[69] Dissolution pores form in chemically unstable minerals, such as feldspar and calcite under acidic fluids modification.[23] Owing to the continuous cracking, conversion, and migration of OM, not only are OM pores formed in different kinds of organic matter but also some hydrocarbons fill in various types of interconnected pores in the shale (Figure 19c,d).[22,50,68,70−72] In addition, the pore pressure in the shale increases due to the accumulation of hydrocarbons.[50,65] Notably, more hydrocarbons in the open system were expelled through the unconformity to be stored in the Sinian Dengying Formation (Figure 19d). Hence, the pore pressure of shale in the open system may be relatively lower than that in the semiopen system.

In the overmature stage, more gas and OM pores developed in organic-rich shales.[50,64,68] The pore pressures inside the two sealing systems appear significantly different because of the enormous difference between the oil and gas volumes.[66] In the later overmature stage, some rigid frameworks gradually lose the protective effect with increased burial depth and overlying formation pressure but still protect the pores by the pressure shadow to some extent (Figure 19e). Moreover, the pore pressure gradually decreased because the quantity of hydrocarbon expulsion exceeded that of hydrocarbon generation. Therefore, the stress equilibrium state between pore pressure and external stress was progressively disrupted. The size and morphology of the OM pores varied continuously with the changes in the stress equilibrium state. Compared to the semiopen system, the open system had a poorer sealing capacity and higher hydrocarbon expulsion efficiency, resulting in a faster pore pressure decrease and OM pores being small, flat, or slitlike (Figure 19f).

## 6. CONCLUSIONS

(1) Feldspar and OM−mineral aggregates (e.g., OM−clay, OM−rutile, and OM−apatite aggregates) provided various pores to the shale and influenced the relative proportions of surface porosity for different types of pores but also preserved the pores to some extent with a rigid framework and pressure shadow.

(2) The sealing capacity of the floor affects the hydrocarbon expulsion efficiency and pore pressure of the Qiongzhusi Formation in different sealing systems. During thermal evolution, the quantity of hydrocarbon generation controlled by OM decomposition and the quantity of hydrocarbon expulsion controlled by the sealing system together affect the variation in pore pressure and the stress equilibrium state between pore pressure and external stresses in the shale. Consequently, the characteristics of pore development change continuously with variations in the stress equilibrium state. Once the stress equilibrium state was disrupted, the OM pores deformed, narrowed, or even closed under the influence of compaction owing to the loss of overpressure protection.

(3) The pore characteristics of the Qiongzhusi Formation shales responded significantly to different sealing systems. The open system had a few OM pores that were flat and slitlike, whereas the semiopen system had more round and elliptical OM pores. Meanwhile, the open system had the smallest average diameter of the OM pores, approximately 40.2% smaller than that of the semiopen system. Furthermore, the pore volume and specific surface area of the mesopores for the shales in the open system were reduced by 38.4% and 37.7%, respectively, compared to the semiopen system.

## AUTHOR INFORMATION


### Corresponding Authors

**Wen Zhou** − *State Key Laboratory of Oil and Gas Reservoir Geology and Exploitation and College of Energy, Chengdu University of Technology, Chengdu, Sichuan 610059, China;* orcid.org/0000-0003-0479-631X; Email: zhouw62@cdut.edu.cn

**Hao Xu** − *State Key Laboratory of Oil and Gas Reservoir Geology and Exploitation and College of Energy, Chengdu University of Technology, Chengdu, Sichuan 610059, China;* orcid.org/0000-0001-8412-1309; Email: haoxu777@qq.com

### Authors

**Ruiyin Liu** − *State Key Laboratory of Oil and Gas Reservoir Geology and Exploitation and College of Energy, Chengdu University of Technology, Chengdu, Sichuan 610059, China;* orcid.org/0000-0002-5729-3583

**Qiumei Zhou** − *State Key Laboratory of Oil and Gas Reservoir Geology and Exploitation and College of Energy, Chengdu University of Technology, Chengdu, Sichuan 610059, China*




https://doi.org/10.1021/acsomega.2c00869
ACS Omega 2022, 7, 15821−15840

**Ke Jiang** − *State Key Laboratory of Oil and Gas Reservoir Geology and Exploitation and College of Energy, Chengdu University of Technology, Chengdu, Sichuan 610059, China*
**Fuhua Shang** − *Key Laboratory of Coal Bed Methane Resource & Reservoir Formation Process, Ministry of Education, China University of Mining and Technology, Xuzhou 221008, China;* orcid.org/0000-0003-2134-9183
**Wenlu Gao** − *State Key Laboratory of Oil and Gas Reservoir Geology and Exploitation and College of Energy, Chengdu University of Technology, Chengdu, Sichuan 610059, China*
**Weiguo Song** − *State Key Laboratory of Oil and Gas Reservoir Geology and Exploitation and College of Energy, Chengdu University of Technology, Chengdu, Sichuan 610059, China*
**Dongxu Liu** − *State Key Laboratory of Oil and Gas Reservoir Geology and Exploitation and College of Energy, Chengdu University of Technology, Chengdu, Sichuan 610059, China*
**Hongshuai Zhao** − *State Key Laboratory of Oil and Gas Reservoir Geology and Exploitation and College of Energy, Chengdu University of Technology, Chengdu, Sichuan 610059, China*
**Xin Zhao** − *State Key Laboratory of Oil and Gas Reservoir Geology and Exploitation and College of Energy, Chengdu University of Technology, Chengdu, Sichuan 610059, China*

Complete contact information is available at: https://pubs.acs.org/10.1021/acsomega.2c00869

### Notes

The authors declare no competing financial interest.

## ■ ACKNOWLEDGMENTS

The authors thank the National Natural Science Foundation of China (Grant Nos. 41972137 and 42002157) and Sichuan Science and Technology Support Project (2021YJ0349) for financial assistance to this research.

## ■ REFERENCES

(1) Zou, C.; Dong, D.; Wang, Y.; Li, X.; Huang, J.; Wang, S.; Guan, Q.; Zhang, C.; Wang, H.; Liu, H.; Bai, W.; Liang, F.; Lin, W.; Zhao, Q.; Liu, D.; Yang, Z.; Liang, P.; Sun, S.; Qiu, Z. Shale gas in China: Characteristics, challenges and prospects (I). *Petroleum Exploration and Development* **2015**, *42* (6), 753−767.
(2) Ma, X.; Xie, J. The progress and prospects of shale gas exploration and development in southern Sichuan Basin, SW China. *Petroleum Exploration and Development* **2018**, *45* (1), 172−182.
(3) Jiang, Z.; Song, Y.; Tang, X.; Li, Z.; Wang, X.; Wang, G.; Xue, Z.; Li, X.; Zhang, K.; Chang, J.; Qiu, H. Controlling factors of marine shale gas differential enrichment in southern China. *Petroleum Exploration and Development* **2020**, *47* (3), 661−673.
(4) Zou, C.; Dong, D.; Wang, Y.; Li, X.; Huang, J.; Wang, S.; Guan, Q.; Zhang, C.; Wang, H.; Liu, H.; Bai, W.; Liang, F.; Lin, W.; Zhao, Q.; Liu, D.; Yang, Z.; Liang, P.; Sun, S.; Qiu, Z. Shale gas in China: Characteristics, challenges and prospects (II). *Petroleum Exploration and Development* **2016**, *43* (2), 182−196.
(5) Shang, F.; Zhu, Y.; Hu, Q.; Wang, Y.; Li, Y.; Li, W.; Liu, R.; Gao, H. Factors controlling organic-matter accumulation in the Upper Ordovician-Lower Silurian organic-rich shale on the northeast margin of the Upper Yangtze platform: Evidence from petrographic and geochemical proxies. *Mar. Petrol. Geol.* **2020**, *121*, 104597.
(6) Xu, H.; Zhou, W.; Cao, Q.; Xiao, C.; Zhou, Q.; Zhang, H.; Zhang, Y. Differential fluid migration behaviour and tectonic movement in Lower Silurian and Lower Cambrian shale gas systems in China using isotope geochemistry. *Mar. Petrol. Geol.* **2018**, *89*, 47−57.
(7) Shang, F.; Zhu, Y.; Hu, Q.; Zhu, Y.; Wang, Y.; Du, M.; Liu, R.; Han, Y. Characterization of methane adsorption on shale of a complex tectonic area in Northeast Guizhou, China: Experimental results and geological significance. *J. Nat. Gas Sci. Eng.* **2020**, *84*, 103676.
(8) Ross, D. J. K.; Marc Bustin, R. The importance of shale composition and pore structure upon gas storage potential of shale gas reservoirs. *Mar. Petrol. Geol.* **2009**, *26* (6), 916−927.
(9) Wang, Y.; Liu, L.; Cheng, H. Gas Adsorption Characterization of Pore Structure of Organic-rich Shale: Insights into Contribution of Organic Matter to Shale Pore Network. *Natural Resources Research* **2021**, *30* (3), 2377−2395.
(10) Passey, Q. R.; Bohacs, K. M.; Esch, W. L.; Klimentidis, R.; Sinha, S. From oil-prone source rock to gas-producing shale reservoir−geologic and petrophysical characterization of unconventional shale-gas reservoirs. In *International oil and gas conference and exhibition in China*, Beijing, China, 2010-06-08; SPO Engineers, Eds.; OnePetro: Beijing, China, 2010; pp 6−34. DOI: 10.2118/131350-MS.
(11) Xu, H.; Zhou, W.; Hu, Q.; Xia, X.; Zhang, C.; Zhang, H. Fluid distribution and gas adsorption behaviors in over-mature shales in southern China. *Mar. Petrol. Geol.* **2019**, *109*, 223−232.
(12) Jarvie, D. M.; Hill, R. J.; Ruble, T. E.; Pollastro, R. M. Unconventional shale-gas systems: The Mississippian Barnett Shale of north-central Texas as one model for thermogenic shale-gas assessment. *AAPG Bull.* **2007**, *91* (4), 475−499.
(13) Loucks, R. G.; Reed, R. M.; Ruppel, S. C.; Hammes, U. Spectrum of pore types and networks in mudrocks and a descriptive classification for matrix-related mudrock pores. *AAPG Bull.* **2012**, *96* (6), 1071−1098.
(14) Bridge, J.; Demicco, R. *Earth surface processes, landforms and sediment deposits*; Cambridge University Press, 2008.
(15) Zhu, H.; Ju, Y.; Huang, C.; Han, K.; Qi, Y.; Shi, M.; Yu, K.; Feng, H.; Li, W.; Ju, L.; Qian, J. Pore structure variations across structural deformation of Silurian Longmaxi Shale: An example from the Chuandong Thrust-Fold Belt. *Fuel* **2019**, *241*, 914−932.
(16) Ma, Y.; Ardakani, O. H.; Zhong, N.; Liu, H.; Huang, H.; Larter, S.; Zhang, C. Possible pore structure deformation effects on the shale gas enrichment: An example from the Lower Cambrian shales of the Eastern Upper Yangtze Platform, South China. *Int. J. Coal Geol.* **2020**, *217*, 103349.
(17) Shang, F.; Zhu, Y.; Gao, H.; Wang, Y.; Liu, R. Relationship between Tectonism and Composition and Pore Characteristics of Shale Reservoirs. *Geofluids* **2020**, *2020*, 1−14.
(18) Gou, Q.; Xu, S.; Hao, F.; Yang, F.; Shu, Z.; Liu, R. The effect of tectonic deformation and preservation condition on the shale pore structure using adsorption-based textural quantification and 3D image observation. *Energy* **2021**, *219*, 119579.
(19) Bernard, S.; Horsfield, B.; Schulz, H.; Wirth, R.; Schreiber, A.; Sherwood, N. Geochemical evolution of organic-rich shales with increasing maturity: A STXM and TEM study of the Posidonia Shale (Lower Toarcian, northern Germany). *Mar. Petrol. Geol.* **2012**, *31* (1), 70−89.
(20) Bernard, S.; Wirth, R.; Schreiber, A.; Schulz, H.; Horsfield, B. Formation of nanoporous pyrobitumen residues during maturation of the Barnett Shale (Fort Worth Basin). *Int. J. Coal Geol.* **2012**, *103*, 3−11.
(21) Cardott, B. J.; Landis, C. R.; Curtis, M. E. Post-oil solid bitumen network in the Woodford Shale, USA — A potential primary migration pathway. *Int. J. Coal Geol.* **2015**, *139*, 106−113.
(22) Löhr, S. C.; Baruch, E. T.; Hall, P. A.; Kennedy, M. J. Is organic pore development in gas shales influenced by the primary porosity and structure of thermally immature organic matter? *Org. Geochem.* **2015**, *87*, 119−132.
(23) Schieber, J. Common themes in the formation and preservation of intrinsic porosity in shales and mudstones−illustrated with examples across the Phanerozoic. In *SPE Unconventional Gas Conference*, Pittsburgh, PA, 2010-02-23; OnePetro: Pittsburgh, PA, 2010. DOI: 10.2118/132370-MS.

(24) Guo, X.; Hu, D.; Li, Y.; Wei, Z.; Wei, X.; Liu, Z. Geological factors controlling shale gas enrichment and high production in Fuling shale gas field. *Petroleum Exploration and Development* **2017**, *44* (4), 513−523.
(25) Hu, D.; Zhang, H.; Ni, K.; Yu, G. Preservation conditions for marine shale gas at the southeastern margin of the Sichuan Basin and their controlling factors. *Natural Gas Industry B* **2014**, *1* (2), 178−184.
(26) Milliken, K. L.; Rudnicki, M.; Awwiller, D. N.; Zhang, T. Organic matter-hosted pore system, Marcellus Formation (Devonian), Pennsylvania. *AAPG Bull.* **2013**, *97* (2), 177−200.
(27) Li, X.; Jiang, Z.; Wang, P.; Song, Y.; Li, Z.; Tang, X.; Li, T.; Zhai, G.; Bao, S.; Xu, C.; Wu, F. Porosity-preserving mechanisms of marine shale in Lower Cambrian of Sichuan Basin, South China. *J. Nat. Gas Sci. Eng.* **2018**, *55*, 191−205.
(28) Jiao, K.; Ye, Y.; Liu, S.; Ran, B.; Deng, B.; Li, Z.; Li, J.; Yong, Z.; Sun, W. Characterization and Evolution of Nanoporosity in Superdeeply Buried Shales: A Case Study of the Longmaxi and Qiongzhusi Shales from MS Well #1, North Sichuan Basin, China. *Energy Fuel.* **2018**, *32* (1), 191−203.
(29) Zhang, K.; Song, Y.; Jia, C.; Jiang, Z.; Jiang, S.; Huang, Y.; Wen, M.; Liu, X.; Liu, W.; Chen, Z.; Xie, X.; Liu, T.; Wang, X.; Wang, P.; Li, X.; Shan, C. Vertical sealing mechanism of shale and its roof and floor and effect on shale gas accumulation, a case study of marine shale in Sichuan basin, the Upper Yangtze area. *J. Petrol. Sci. Eng.* **2019**, *175*, 743−754.
(30) Jin, Z.; Nie, H.; Liu, Q.; Zhao, J.; Jiang, T. Source and seal coupling mechanism for shale gas enrichment in upper Ordovician Wufeng Formation - Lower Silurian Longmaxi Formation in Sichuan Basin and its periphery. *Mar. Petrol. Geol.* **2018**, *97*, 78−93.
(31) Liu, S.; Yang, Y.; Deng, B.; Zhong, Y.; Wen, L.; Sun, W.; Li, Z.; Jansa, L.; Li, J.; Song, J.; Zhang, X.; Peng, H. Tectonic evolution of the Sichuan Basin, Southwest China. *Earth-Sci. Rev.* **2021**, *213*, 103470.
(32) Xu, H.; Zhou, W.; Zhang, R.; Liu, S.; Zhou, Q. Characterizations of pore, mineral and petrographic properties of marine shale using multiple techniques and their implications on gas storage capability for Sichuan Longmaxi gas shale field in China. *Fuel* **2019**, *241*, 360−371.
(33) Tian, S.; Bowen, L.; Liu, B.; Zeng, F.; Xue, H.; Erastova, V.; Chris Greenwell, H.; Dong, Z.; Zhao, R.; Liu, J. A method for automatic shale porosity quantification using an Edge-Threshold Automatic Processing (ETAP) technique. *Fuel* **2021**, *304*, 121319.
(34) Deng, H.; Hu, X.; Li, H. A.; Luo, B.; Wang, W. Improved pore-structure characterization in shale formations with FESEM technique. *J. Nat. Gas Sci. Eng.* **2016**, *35*, 309−319.
(35) Liu, B.; Gao, Y.; Liu, K.; Liu, J.; Ostadhassan, M.; Wu, T.; Li, X. Pore structure and adsorption hysteresis of the middle Jurassic Xishanyao shale formation in the Southern Junggar Basin, northwest China. *Energy Explor. Exploit.* **2021**, *39* (3), 761−778.
(36) Avnir, D.; Jaroniec, M. An isotherm equation for adsorption on fractal surfaces of heterogeneous porous materials. *Langmuir* **1989**, *5* (6), 1431−1433.
(37) Liu, B.; He, S.; Meng, L.; Fu, X.; Gong, L.; Wang, H. Sealing mechanisms in volcanic faulted reservoirs in Xujiaweizi extension, northern Songliao Basin, northeastern China. *AAPG Bull.* **2021**, *105* (8), 1721−1743.
(38) Tang, L.; Song, Y.; Jiang, S.; Li, L.; Li, Z.; Li, Q.; Yang, Y. Sealing Mechanism of the Roof and Floor for the Wufeng-Longmaxi Shale Gas in the Southern Sichuan Basin. *Energy Fuel.* **2020**, *34* (6), 6999−7018.
(39) Thommes, M.; Kaneko, K.; Neimark, A. V.; Olivier, J. P.; Rodriguez-Reinoso, F.; Rouquerol, J.; Sing, K. S. W. Physisorption of gases, with special reference to the evaluation of surface area and pore size distribution (IUPAC Technical Report). *Pure Appl. Chem.* **2015**, *87* (9−10), 1051−1069.
(40) Sing, K. S. Reporting physisorption data for gas/solid systems with special reference to the determination of surface area and porosity (Recommendations 1984). *Pure Appl. Chem.* **1985**, *57* (4), 603−619.
(41) Curtis, M. E.; Cardott, B. J.; Sondergeld, C. H.; Rai, C. S. Development of organic porosity in the Woodford Shale with increasing thermal maturity. *Int. J. Coal Geol.* **2012**, *103*, 26−31.
(42) Xi, Z.; Tang, S.; Li, J.; Zhang, Z.; Xiao, H. Pore characterization and the controls of organic matter and quartz on pore structure: Case study of the Niutitang Formation of northern Guizhou Province, South China. *J. Nat. Gas Sci. Eng.* **2019**, *61*, 18−31.
(43) Zhao, J.; Jin, Z.; Jin, Z.; Wen, X.; Geng, Y. Origin of authigenic quartz in organic-rich shales of the Wufeng and Longmaxi Formations in the Sichuan Basin, South China: Implications for pore evolution. *J. Nat. Gas Sci. Eng.* **2017**, *38*, 21−38.
(44) Min, H.; Zhang, T.; Li, Y.; Zhao, S.; Li, J.; Lin, D.; Wang, J. The Albitization of K-Feldspar in Organic- and Silt-Rich Fine-Grained Rocks of the Lower Cambrian Qiongzhusi Formation in the Southwestern Upper Yangtze Region, China. *Minerals* **2019**, *9* (10), 620.
(45) Kennedy, M. J.; Löhr, S. C.; Fraser, S. A.; Baruch, E. T. Direct evidence for organic carbon preservation as clay-organic nanocomposites in a Devonian black shale; from deposition to diagenesis. *Earth Planet. Sc. Lett.* **2014**, *388*, 59−70.
(46) Löhr, S. C.; Kennedy, M. J. Organomineral nanocomposite carbon burial during Oceanic Anoxic Event 2. *Biogeosciences* **2014**, *11* (18), 4971−4983.
(47) Liu, R.; Hao, F.; Engelder, T.; Shu, Z.; Yi, J.; Xu, S.; Teng, C. Influence of tectonic exhumation on porosity of Wufeng−Longmaxi shale in the Fuling gas field of the eastern Sichuan Basin, China. *AAPG Bull.* **2020**, *104* (4), 939−959.
(48) Kuila, U.; Prasad, M. Specific surface area and pore-size distribution in clays and shales. *Geophys. Prospect.* **2013**, *61* (2), 341−362.
(49) Milliken, K. L.; Ko, L. T.; Pommer, M.; Marsaglia, K. M. Sem Petrography of Eastern Mediterranean Sapropels: Analogue Data For Assessing Organic Matter In Oil and Gas Shales. *J. Sediment. Res.* **2014**, *84* (11), 961−974.
(50) Ko, L. T.; Ruppel, S. C.; Loucks, R. G.; Hackley, P. C.; Zhang, T.; Shao, D. Pore-types and pore-network evolution in Upper Devonian-Lower Mississippian Woodford and Mississippian Barnett mudstones: Insights from laboratory thermal maturation and organic petrology. *Int. J. Coal Geol.* **2018**, *190*, 3−28.
(51) Xu, S.; Gou, Q.; Hao, F.; Zhang, B.; Shu, Z.; Lu, Y.; Wang, Y. Shale pore structure characteristics of the high and low productivity wells, Jiaoshiba shale gas field, Sichuan Basin, China: Dominated by lithofacies or preservation condition? *Mar. Petrol. Geol.* **2020**, *114*, 104211.
(52) Xiong, L.; Ge, Z.; Wang, T.; Wen, Z.; Zhong, W.; Zhou, H.; He, X., Exploration potential of Cambrian Qiongzhusi Formation in southern Sichuan Basin. *Reservoir Evaluation and Development* **2021**, *11* (1), 14−21, 55 (in Chinese with English abstract). .
(53) Zhang, L.; Xiao, D.; Lu, S.; Jiang, S.; Chen, L.; Guo, T.; Wu, L. Pore development of the Lower Longmaxi shale in the southeastern Sichuan Basin and its adjacent areas: Insights from lithofacies identification and organic matter. *Mar. Petrol. Geol.* **2020**, *122*, 104662.
(54) Wei, S.; He, S.; Pan, Z.; Zhai, G.; Dong, T.; Guo, X.; Yang, R.; Han, Y.; Yang, W. Characteristics and evolution of pyrobitumen-hosted pores of the overmature Lower Cambrian Shuijingtuo Shale in the south of Huangling anticline, Yichang area, China: Evidence from FE-SEM petrography. *Mar. Petrol. Geol.* **2020**, *116*, 104303.
(55) Yang, W.; Zuo, R.; Jiang, Z.; Chen, D.; Song, Y.; Luo, Q.; Wang, Q.; Zhu, H. Effect of lithofacies on pore structure and new insights into pore-preserving mechanisms of the over-mature Qiongzhusi marine shales in Lower Cambrian of the southern Sichuan Basin, China. *Mar. Petrol. Geol.* **2018**, *98*, 746−762.
(56) Wang, G. Deformation of organic matter and its effect on pores in mud rocks. *AAPG Bul.* **2020**, *103* (1), 21−36.
(57) Eliyahu, M.; Emmanuel, S.; Day-Stirrat, R. J.; Macaulay, C. I. Mechanical properties of organic matter in shales mapped at the nanometer scale. *Mar. Petrol. Geol.* **2015**, *59*, 294−304.


https://doi.org/10.1021/acsomega.2c00869
*ACS Omega* 2022, 7, 15821−15840

(58) Kumar, V.; Sondergeld, C.; Rai, C. S. Effect of mineralogy and organic matter on mechanical properties of shale. *Interpretation* **2015**, *3* (3), SV9−SV15.
(59) Labani, M. M.; Rezaee, R. The Importance of Geochemical Parameters and Shale Composition on Rock Mechanical Properties of Gas Shale Reservoirs: a Case Study From the Kockatea Shale and Carynginia Formation From the Perth Basin, Western Australia. *Rock Mech. Rock Eng.* **2015**, *48* (3), 1249−1257.
(60) Liu, S.; Li, Z.; Deng, B.; Sun, W.; Li, Z.; Ding, Y.; Song, J.; Wu, J. Occurrence morphology of bitumen in Dengying Formation deep and ultra-deep carbonate reservoirs of the Sichuan Basin and its indicating significance to oil and gas reservoirs. *Natural Gas Industry B* **2022**, *9* (1), 73−83 (in Chinese with English abstract)..
(61) Li, X.; Jiang, Z.; Song, Y.; Zhai, G.; Bao, S.; Li, Z.; Tang, X.; Wang, P.; Li, T.; Wang, G.; Zhou, W.; Qiu, H.; Miao, Y. Porosity evolution mechanisms of marine shales at over-maturity stage: Insight from comparable analysis between Lower Cambrian and Lower Silurian inside and at the margin of the Sichuan Basin, South China. *Interpretation* **2018**, *6* (3), T739−T757.
(62) Sun, W.; Shugen, L.; Yongsheng, M.; Xunyu, C.; Guosheng, X.; Guozhi, W.; Ziquan, Y.; Haifeng, Y.; Changlin, P. Determination and Quantitative Simulation of Gas Pool Formation Process of Sinian Cracked Gas in Weiyuan—Ziyang Area, Sichuan Basin. *ACTA GEOLOGICA SINICA* **2007**, *81* (08), 1153−1159 (in Chinese with English abstract). CNKI:SUN:DZXE.0.2007-08-015..
(63) Liu, Y.; Xiong, Y.; Li, Y.; Peng, P. Effect of thermal maturation on chemical structure and nanomechanical properties of solid bitumen. *Mar. Petrol. Geol.* **2018**, *92*, 780−793.
(64) Ko, L. T.; Loucks, R. G.; Zhang, T.; Ruppel, S. C.; Shao, D. Pore and pore network evolution of Upper Cretaceous Boquillas (Eagle Ford−equivalent) mudrocks: Results from gold tube pyrolysis experiments. *AAPG Bull.* **2016**, *100* (11), 1693−1722.
(65) Tissot, B. P.; Pelet, R.; Ungerer, P. Thermal history of sedimentary basins, maturation indices, and kinetics of oil and gas generation. *AAPG Bull.* **1987**, *71* (12), 1445−1466.
(66) Liu, J.; Liu, T.; Liu, H.; He, L.; Zheng, L. Overpressure caused by hydrocarbon generation in the organic-rich shales of the Ordos Basin. *Mar. Petrol. Geol.* **2021**, *134*, 105349.
(67) Liu, W.; Qiu, N.; Xu, Q.; Chang, J. The quantitative evaluation of the pressurization caused by hydrocarbon generation in the Cambrian Qiongzhusi Formation of the Gaoshiti-Moxi area, Sichuan Basin. *Petroleum Science Bulletin* **2018**, *3* (3), 262−271 (in Chinese with English abstract)..
(68) Mastalerz, M.; Schimmelmann, A.; Drobniak, A.; Chen, Y. Porosity of Devonian and Mississippian New Albany Shale across a maturation gradient: Insights from organic petrology, gas adsorption, and mercury intrusion. *AAPG Bull.* **2013**, *97* (10), 1621−1643.
(69) Emmings, J. F.; Dowey, P. J.; Taylor, K. G.; Davies, S. J.; Vane, C. H.; Moss-Hayes, V.; Rushton, J. C. Origin and implications of early diagenetic quartz in the Mississippian Bowland Shale Formation, Craven Basin, UK. *Mar. Petrol. Geol.* **2020**, *120*, 104567.
(70) Jiang, K.; Zhou, W.; Deng, N.; Song, W. Statistical analysis and significance of pyrite in the Wufeng-Lower Longmaxi Shale Formation in South China. *Arab. J. Geosci.* **2020**, DOI: 10.1007/s12517-020-06190-0.
(71) Wu, J.; Liang, C.; Yang, R.; Xie, J. The significance of organic matter−mineral associations in different lithofacies in the Wufeng and longmaxi shale-gas reservoirs in the Sichuan Basin. *Mar. Petrol. Geol.* **2021**, *126*, 104866.
(72) Zargari, S.; Canter, K. L.; Prasad, M. Porosity evolution in oil-prone source rocks. *Fuel* **2015**, *153*, 110−117.



https://doi.org/10.1021/acsomega.2c00869
*ACS Omega* 2022, 7, 15821−15840